

Block-wise Primal-dual Algorithms for Large-scale Doubly Penalized ANOVA Modeling

Penghui Fu¹ and Zhiqiang Tan¹

October 21, 2022

Abstract. For multivariate nonparametric regression, doubly penalized ANOVA modeling (DPAM) has recently been proposed, using hierarchical total variations (HTVs) and empirical norms as penalties on the component functions such as main effects and multi-way interactions in a functional ANOVA decomposition of the underlying regression function. The two penalties play complementary roles: the HTV penalty promotes sparsity in the selection of basis functions within each component function, whereas the empirical-norm penalty promotes sparsity in the selection of component functions. We adopt backfitting or block minimization for training DPAM, and develop two suitable primal-dual algorithms, including both batch and stochastic versions, for updating each component function in single-block optimization. Existing applications of primal-dual algorithms are intractable in our setting with both HTV and empirical-norm penalties. Through extensive numerical experiments, we demonstrate the validity and advantage of our stochastic primal-dual algorithms, compared with their batch versions and a previous active-set algorithm, in large-scale scenarios.

Key words and phrases. ANOVA modeling; Nonparametric regression; Penalized estimation; Primal-dual algorithms; Stochastic algorithms; Stochastic gradient methods; Total variation.

¹Department of Statistics, Rutgers University. Address: 110 Frelinghuysen Road, Piscataway, NJ 08854. E-mails: penghui.fu@rutgers.edu, ztan@stat.rutgers.edu.

1 Introduction

Consider functional analysis-of-variance (ANOVA) modeling for multivariate nonparametric regression (e.g., Gu (2013)). Let Y_i and $X_i = (X_{i1}, \dots, X_{ip})^\top$, $i = 1, \dots, n$, be a collection of independent observations of a response variable and a covariate vector. For continuous responses, nonparametric regression can be stated such that

$$Y_i = f(X_{i1}, \dots, X_{ip}) + \varepsilon_i, \quad (1)$$

where $f(x) = f(x_1, \dots, x_p)$ is an unknown function, and ε_i is a noise with mean zero and a finite variance given X_i . In the framework of functional ANOVA modeling, the multivariate function f is decomposed as

$$\begin{aligned} f(x_1, \dots, x_p) = & f_0 + \sum_{1 \leq j_1 \leq p} f_{j_1}(x_{j_1}) + \sum_{1 \leq j_1 < j_2 \leq p} f_{j_1, j_2}(x_{j_1}, x_{j_2}) + \dots \\ & + \sum_{1 \leq j_1 < \dots < j_K \leq p} f_{j_1, \dots, j_K}(x_{j_1}, \dots, x_{j_K}), \end{aligned} \quad (2)$$

where f_0 is a constant, f_{j_1} 's are univariate functions representing main effects, f_{j_1, j_2} 's are bivariate functions representing two-way interactions, etc, and K is the maximum way of interactions allowed. The special case of (1)–(2) with $K = 1$ is known as additive modeling (Stone, 1986; Hastie & Tibshirani, 1990). For general $K \geq 2$, a notable example is smoothing spline ANOVA modeling (Wahba et al., 1995; Lin & Zhang, 2006; Gu, 2013), where the component functions in (2) are assumed to lie in tensor-product reproducing kernel Hilbert spaces (RKHSs), defined from univariate Sobolev- L_2 spaces as in smoothing splines. Alternatively, in Yang & Tan (2021), a class of hierarchical total variations (HTVs) is introduced to measure roughness of main effects and multi-way interactions by properly extending the total variation associated with the univariate Sobolev- L_1 space. Compared with smoothing spline ANOVA modeling, this approach extends univariate regression splines using total variation penalties (Mammen & Van De Geer, 1997).

Recently, theory and methods have been expanded for additive and ANOVA modeling to high-dimensional settings, with p close to or greater than n . Examples include Ravikumar et al. (2009), Meier et al. (2009), Koltchinskii & Yuan (2010), Radchenko & James (2010), Raskutti et al. (2012), Petersen et al. (2016), Tan & Zhang (2019), and Yang & Tan (2018, 2021) among others. An important idea from the high-dimensional methods is to employ

empirical L_2 norms of component functions as penalties, in addition to functional semi-norms which measure roughness of the component functions, such as the Sobolev- L_2 semi-norm or total variation for univariate functions in the case of additive modeling ($K = 1$). For $K \geq 2$, the incorporation of empirical-norm penalties is relevant even when p is relatively small against n , because the total number of component functions in (2) scales as p^K .

In this work, we are interested in doubly penalized ANOVA modeling (DPAM) in Yang & Tan (2021), using both the HTVs and empirical L_2 norms as penalties on the component functions in (2). To describe the method, the ANOVA decomposition (2) can be expressed in a more compact notation as

$$f(x_1, \dots, x_p) = f_0 + \sum_{S_1:|S_1|=1} f_{S_1} + \sum_{S_2:|S_2|=2} f_{S_2} + \dots + \sum_{S_K:|S_K|=K} f_{S_K}, \quad (3)$$

where S_k is a subset of size k from $\{1, \dots, p\}$ for $k = 1, \dots, K$, and $f_{S_k} = f_{j_1, \dots, j_k}(x_{j_1}, \dots, x_{j_k})$ if $S_k = \{j_1, \dots, j_k\}$. For identifiability, the component functions are assumed to be uniquely defined as $f_{S_k} = (\prod_{j \in S_k} (I - H_j) \prod_{j \notin S_k} H_j) f$, where H_j is a marginalization operator over x_j , for example, defined by averaging over X_{ij} 's in the training set. For $m \geq 1$, the HTV of differentiation order m , denoted as HTV^m , is defined inductively in m . For example, for a univariate function $f = f(x_1)$, $\text{HTV}^1(f) = \text{TV}(f)$ and $\text{HTV}^2(f) = \text{HTV}(D_1 f)$, where D_1 is the differentiation operator in x_1 and TV is the standard total variation as in Mammen & Van De Geer (1997). For a bivariate function $f = f(x_1, x_2)$, the HTV with $m = 1$ or 2 is considerably more complicated (even after ignoring scaling constants):

$$\begin{aligned} \text{HTV}^1(f) &= \text{TV}(f_{12}) + \text{TV}(f_1) + \text{TV}(f_2), \\ \text{HTV}^2(f) &= \text{HTV}^1(D_1 D_2 f_{12}) + \text{HTV}^1(D_1 f_1) + \text{HTV}^1(D_2 f_2), \end{aligned}$$

where (f_1, f_2, f_{12}) are the component functions in the ANOVA decomposition (3). Nevertheless, suitable basis functions are derived in Yang & Tan (2021) to achieve the following properties in a set of multivariate splines, defined as the union of all tensor products of up to K sets of univariate splines, depending on differentiation order m and pre-specified marginal knots over each coordinate. First, the ANOVA decomposition (3) for such a multivariate spline f can be represented as

$$f = \beta_0 + \sum_{k=1}^K \sum_{S_k:|S_k|=k} \Psi_{S_k}^T \beta_{S_k}, \quad (4)$$

with $f_0 = \beta_0$ and $f_{S_k} = \Psi_{S_k}^T \beta_{S_k}$, where Ψ_{S_k} is the basis vector in $(x_{j_1}, \dots, x_{j_k})$ and β_{S_k} is the associated coefficient vector for $S_k = \{j_1, \dots, j_k\}$ and $k = 1, \dots, K$. Moreover, the HTV can be transformed into a Lasso representation, with $\text{HTV}^m(f_{S_k}) = \|\Gamma_{S_k} \beta_{S_k}\|_1$:

$$\text{HTV}^m(f) = \sum_{k=1}^K \sum_{S_k: |S_k|=k} \|\Gamma_{S_k} \beta_{S_k}\|_1, \quad (5)$$

where $\|\cdot\|_1$ denotes the L_1 norm of a vector, ρ_k is a scaling constant for HTV of k -variate component f_{S_k} , and Γ_{S_k} is a diagonal matrix with each diagonal element either 0 or ρ_k (with 0 indicating that the corresponding element of β_{S_k} is not penalized, for example, the coefficient of a fully linear basis in the case of $m = 2$). For $m = 1$ or 2, the univariate spline bases are piecewise constant or linear, and the resulting multivariate spline bases are, respectively, piecewise constant or cross-linear (i.e., being piecewise linear in each coordinate with all other coordinates fixed). Readers are referred to Yang & Tan (2021) for further details, although such details are not required in our subsequent discussion.

With the preceding background, linear DPAM is defined by solving

$$\min_{\beta} \frac{1}{2} \|Y - f\|_n^2 + \sum_{k=1}^K \sum_{S_k: |S_k|=k} \left(\text{HTV}^m(f_{S_k}) + \lambda_k \|f_{S_k}\|_n \right),$$

or, with the representations (4) and (5), by solving

$$\min_{\beta} \frac{1}{2} \left\| Y - \beta_0 - \sum_{k=1}^K \sum_{S_k: |S_k|=k} \Psi_{S_k}^T \beta_{S_k} \right\|_n^2 + \sum_{k=1}^K \sum_{S_k: |S_k|=k} \left(\|\Gamma_{S_k} \beta_{S_k}\|_1 + \lambda_k \|\Psi_{S_k}^T \beta_{S_k}\|_n \right), \quad (6)$$

where β consists of β_0 and $(\beta_{S_k})_{k, S_k}$, $\|\cdot\|_n$ denotes the empirical L_2 norm (or in short, empirical norm), e.g., $\|f\|_n = \{n^{-1} \sum_{i=1}^n f^2(X_i)\}^{1/2}$, and λ_k is a tuning parameter for $k = 1, \dots, K$. As reflected in the name DPAM, there are two penalty terms involved, the HTV $\|\Gamma_{S_k} \beta_{S_k}\|_1$ and the empirical norm $\lambda_k \|\Psi_{S_k}^T \beta_{S_k}\|_n$, which play different roles in promoting sparsity; see Proposition 2 and related discussion. The HTV penalty promotes sparsity among the elements of β_{S_k} (or the selection of basis functions) for each block S_k , whereas the empirical-norm penalty promotes sparsity among the coefficient vectors β_{S_k} (or the component functions f_{S_k}) across S_k . The use of these two penalties is also instrumental in the theory for doubly penalized estimation in additive or ANOVA modeling (Tan & Zhang, 2019).

For binary outcomes, replacing (1) by (nonparametric) logistic regression, $P(Y_i = 1|X_i) = \{1 + \exp(-f(X_i))\}^{-1}$, and the square loss in (6) by the likelihood loss (or cross-entropy) leads

to logistic DPAM, which solves

$$\min_{\beta} \frac{1}{n} \sum_{i=1}^n l\left(Y_i, \beta_0 + \sum_{k, S_k} \Psi_{i, S_k}^T \beta_{S_k}\right) + \sum_{k, S_k} \left(\|\Gamma_{S_k} \beta_{S_k}\|_1 + \lambda_k \|\Psi_{S_k} \beta_{S_k}\|_n\right), \quad (7)$$

where $Y_i \in \{0, 1\}$, $\Psi_{i, S_k} = \Psi_{S_k}(X_{i, j_1}, \dots, X_{i, j_k})$ for $S_k = \{j_1, \dots, j_k\}$, and $l(y, f) = \log(1 + \exp(f)) - yf$ is the likelihood loss for logistic regression.

We develop new optimization algorithms for solving (6) and (7), including stochastic algorithms adaptive to large-scale scenarios (with large sample size n). Similarly as in the earlier literature (Hastie & Tibshirani, 1990), the top-level idea is backfitting or block minimization: the objective is optimized with respect to one block β_{S_k} at a time while fixing the remaining blocks. This approach is valid for solving (6) and (7) due to the block-wise separability of non-differentiable terms (Tseng, 1988). In Yang & Tan (2018, 2021), a backfitting algorithm, called AS-BDT (active-set block descent and thresholding), is proposed by exploiting two supportive properties. First, in the subproblem with respect to only β_{S_k} , the solution can be obtained by jointly soft-thresholding an (exact) solution to the Lasso subproblem with only the penalty $\|\Gamma_{S_k} \beta_{S_k}\|_1$; see Proposition 2. Second, the desired Lasso solution can be computed using an active-set descent algorithm (Osborne et al., 2000), which tends to be efficient when the training dataset is relatively small or the Lasso solution is sufficiently sparse within each block. However, AS-BDT is not designed to efficiently handle large datasets, especially in applications with non-sparse blocks.

As a large-scale alternative to AS-BDT, we investigate primal-dual algorithms, including both batch and stochastic versions, for solving the single-block subproblems in (6) and (7). (We also study a new majorization-minimization algorithm, which is presented in the Supplement.) The primal-dual methods have been extensively studied for large-scale convex optimization, as shown in the book Ryu & Yin (2022). However, existing applications of primal-dual algorithms are intractable in our setting, with both HTV/Lasso and empirical-norm penalties. In particular, SPDC (stochastic primal-dual coordinate method) in Zhang & Xiao (2017) can be seen as a stochastic version of the Chambolle–Pock (CP) algorithm (Esser et al., 2010; Chambolle & Pock, 2011). But SPDC requires the objective to be split into an empirical risk term (f -term), for example, the square loss in (6), and a penalty term (g -term) such that its proximal mapping can be easily evaluated. Such a choice would combine the HTV/Lasso and empirical-norm penalties into a single penalty term, for which

the proximal mapping is numerically intractable to evaluate.

To overcome this difficulty, we formulate a suitable split of the objective into f - and g -terms in our setting with HTV/Lasso and empirical-norm penalties, and derive two tractable primal-dual batch algorithms for solving the DPAM single-block problems. The two algorithms are new applications of, respectively, the CP algorithm and a linearized version of AMA (alternating minimization algorithm) (Tseng, 1991). Furthermore, we propose two corresponding stochastic primal-dual algorithms, with per-iteration cost about $1/n$ of that in the batch algorithms. In contrast with SPDC (where exact unbiased updates are feasible with a separable f -term), our stochastic algorithms are derived by allowing approximately unbiased updates, due to non-separability of the f -term in our split formulation. We demonstrate the validity and effectiveness of our stochastic algorithms in extensive numerical experiments, while leaving formal analysis of convergence to future work.

2 Primal-dual algorithms: Review and new finding

2.1 Notation

We introduce basic concepts and notations, mostly following Ryu & Yin (2022). For a closed, convex and proper (CCP) function f , we denote its Fenchel conjugate as $f^*(y) = \sup_x \{y^\top x - f(x)\}$. If f is CCP then f^* is CCP and $f^{**} = f$. Denote as $\operatorname{argmin}_x f(x)$ the set of minimizers of f . For a CCP f , we denote its proximal mapping as $\mathbf{prox}_f(x) = \operatorname{argmin}_u \frac{1}{2}\|u - x\|_2^2 + f(u)$. If f is CCP, then $\mathbf{prox}_f(x)$ is uniquely defined on the whole space. An important property of proximal mapping is the Moreau's identity

$$\mathbf{prox}_{\alpha f^*}(x) = x - \alpha \cdot \mathbf{prox}_{f/\alpha}(x/\alpha), \quad (8)$$

for $\alpha > 0$ and CCP f . A differentiable function (not necessarily convex) is called L -smooth if its gradient is L -Lipschitz continuous. A differentiable function f is called μ -strongly convex if there exists $\mu > 0$ such that for all x and y , $f(y) \geq f(x) + \nabla f(x)^\top(y - x) + (\mu/2)\|y - x\|_2^2$. It is known that a CCP f is μ -strongly convex if and only if f^* is $(1/\mu)$ -smooth.

Consider an optimization problem in the form

$$\min_x f(Ax) + g(x), \quad (9)$$

or, equivalently, in its split form,

$$\min_{z,x} f(z) + g(x), \quad \text{subject to} \quad -z + Ax = 0, \quad (10)$$

where $x \in \mathbb{R}^d$, $z \in \mathbb{R}^n$, $A \in \mathbb{R}^{n \times d}$, and f and g are CCP. The (full) Lagrangian associated with problem (10) is

$$L(z, x; u) = f(z) + g(x) + u^T(Ax - z), \quad (11)$$

with $u \in \mathbb{R}^n$. Then the dual problem of (10) is

$$\max_u -(f^*(u) + g^*(-A^T u)), \quad (12)$$

We assume that total duality holds: a primal solution (z^*, x^*) for (10) exists (with $z^* = Ax^*$), a dual solution u^* for (12) exists, and (z^*, x^*, u^*) is a saddle point of (11). By minimizing (11) over z , we obtain the primal-dual Lagrangian

$$L(x; u) = g(x) + u^T Ax - f^*(u). \quad (13)$$

The dual problem associated with (13) is still (12), but the primal problem becomes the unconstrained problem (9), in that $\max_u L(x; u) = f(Ax) + g(x)$ and $\min_x L(x; u) = -(f^*(u) + g^*(-A^T u))$. By construction, (x^*, u^*) is a saddle point of (13) if and only if (Ax^*, x^*, u^*) is a saddle point of (11). The two forms of Lagrangian are used in different scenarios later.

In the following subsections, we review several primal-dual methods which are used in our work, and propose a new method, linearized AMA, which corresponds to a dual version of the PAPC/PDFP²O method (Chen et al., 2013; Drori et al., 2015).

2.2 ADMM, linearized ADMM and Chambolle–Pock

Alternating direction method of multipliers (ADMM) has been well studied (e.g., Boyd et al. (2011)). For solving (10), the ADMM iterations are defined as follows: for $k \geq 0$,

$$z^{k+1} = \operatorname{argmin}_z (f(z) - \langle u^k, z \rangle + (\alpha/2)\|Ax^k - z\|_2^2), \quad (14a)$$

$$x^{k+1} \in \operatorname{argmin}_x (g(x) + \langle A^T u^k, x \rangle + (\alpha/2)\|Ax - z^{k+1}\|_2^2), \quad (14b)$$

$$u^{k+1} = u^k + \alpha(Ax^{k+1} - z^{k+1}), \quad (14c)$$

where $\alpha > 0$ is a step size. After completing the square, (14a) is equivalent to evaluating a proximal mapping of f as shown in (15a). However, (14b) in general does not admit

a closed-form solution. To address this, **linearized ADMM** has been proposed with the following iterations for $k \geq 0$:

$$z^{k+1} = \mathbf{prox}_{f/\alpha}(Ax^k + u^k/\alpha), \quad (15a)$$

$$x^{k+1} = \mathbf{prox}_{\tau g}(x^k - \tau A^\top(u^k + \alpha(Ax^k - z^{k+1}))), \quad (15b)$$

$$u^{k+1} = u^k + \alpha(Ax^{k+1} - z^{k+1}), \quad (15c)$$

where $\tau > 0$ is a step size in addition to α . The iterates $(z^{k+1}, x^{k+1}, u^{k+1})$ can be shown to converge to a saddle point of the full Lagrangian (11) provided $0 < \alpha\tau\|A\|_2^2 \leq 1$, where $\|A\|_2$ denotes the spectral norm of A , i.e., the square root of the largest eigenvalue of $A^\top A$. The method is called linearization because (15b) can be obtained by linearizing the quadratic $\|Ax - z^{k+1}\|_2^2$ in (14b) at x^k with an additional regularization $(1/(\alpha\tau))\|x - x^k\|_2^2$, i.e.,

$$x^{k+1} = \operatorname{argmin}_x (g(x) + \langle A^\top u^k, x \rangle + \alpha \langle A^\top (Ax^k - z^{k+1}), x \rangle + (1/(2\tau))\|x - x^k\|_2^2).$$

Moreover, linearized ADMM (15) can be transformed to the **primal-dual hybrid gradient** (PDHG) or **Chambolle–Pock algorithm** (CP) (Esser et al., 2010; Chambolle & Pock, 2011) with the following iterations for $k \geq 0$:

$$v^{k+1} = \mathbf{prox}_{\alpha f^*}(v^k + \alpha A(2x^k - x^{k-1})), \quad (16a)$$

$$x^{k+1} = \mathbf{prox}_{\tau g}(x^k - \tau A^\top v^{k+1}), \quad (16b)$$

which depend on both (v^k, x^k) and x^{k-1} . In fact, if $u^0 = v^0 + \alpha A(x^0 - x^{-1})$, then the two algorithms can be matched with each other, with the following relationship for $k \geq 0$:

$$v^{k+1} = \mathbf{prox}_{\alpha f^*}(\alpha Ax^k + u^k), \quad (17a)$$

$$u^k = v^k + \alpha A(x^k - x^{k-1}). \quad (17b)$$

See the Supplement for details. Under the same condition $0 < \alpha\tau\|A\|_2^2 \leq 1$, the iterates (x^{k+1}, v^{k+1}) converge to a saddle point of the primal-dual Lagrangian (13).

2.3 Proximal gradient, AMA and linearized AMA

As a prologue, we introduce the method of **proximal gradient**, which can be used to derive AMA. As an extension of gradient descent, the method of proximal gradient is designed to

solve composite optimization in the form $\min_x \tilde{f}(x) + \tilde{g}(x)$, where \tilde{f} and \tilde{g} are CCP, \tilde{f} is differentiable but \tilde{g} may be not. The proximal gradient update is

$$x^{k+1} = \mathbf{prox}_{\alpha\tilde{g}}(x^k - \alpha\nabla\tilde{f}(x^k)). \quad (18)$$

For L -smooth \tilde{f} , if $\alpha \in (0, 2/L)$, then the iterate x^{k+1} can be shown to converge to a minimizer of $\tilde{f}(x) + \tilde{g}(x)$. There are various interpretations for the proximal gradient method (Parikh & Boyd, 2014). In particular, when $\alpha \in (0, 1/L]$, the proximal gradient method can be identified as a majorization-minimization (MM) algorithm, which satisfies a descent property (Hunter & Lange, 2004). By the definition of proximal mapping, the update x^{k+1} in (18) is a minimizer of $\tilde{f}(x, x^k) + \tilde{g}(x)$, where $\tilde{f}(x, x^k) = \tilde{f}(x^k) + \langle x - x^k, \nabla\tilde{f}(x^k) \rangle + \frac{1}{2\alpha}\|x - x^k\|_2^2$. When $\alpha \in (0, 1/L]$, $\tilde{f}(x, x^k)$ is an upper bound (or a majorizing function) for \tilde{f} , and hence the update x^{k+1} leads to an MM algorithm. For $\alpha \in (1/L, 2/L)$, the proximal gradient method is no longer an MM algorithm, although convergence can still be established.

Now return to problem (9). If we further assume that f is μ -strongly convex, then f^* is $(1/\mu)$ -smooth. Applying proximal gradient (18) to the dual problem (12), i.e.,

$$\min_u \underbrace{f^*(u)}_{\tilde{f}(u)} + \underbrace{g^*(-A^T u)}_{\tilde{g}(u)},$$

we obtain the **alternating minimization algorithm** (AMA) (Tseng, 1991):

$$z^{k+1} = \operatorname{argmin}_z (f(z) - \langle u^k, z \rangle) = \nabla f^*(u^k), \quad (19a)$$

$$x^{k+1} \in \operatorname{argmin}_x (g(x) + \langle A^T u^k, x \rangle + (\alpha/2)\|Ax - z^{k+1}\|_2^2), \quad (19b)$$

$$u^{k+1} = u^k + \alpha(Ax^{k+1} - z^{k+1}). \quad (19c)$$

See Ryu & Yin (2022) for details about deriving AMA from proximal gradient. Compared with ADMM (14), a major difference is that there is no quadratic term (the augmented term) in (19a), and z^{k+1} takes a simpler form depending on u^k only.

Similarly as (14b) in ADMM, the step (19b) in AMA is in general difficult to implement. By linearizing (19b) in the same way as (15b), we propose **linearized AMA**:

$$\begin{aligned} z^{k+1} &= \operatorname{argmin}_z (f(z) - \langle u^k, z \rangle) = \nabla f^*(u^k), \\ x^{k+1} &= \mathbf{prox}_{\tau g} (x^k - \tau A^T (u^k + \alpha(Ax^k - z^{k+1}))), \\ u^{k+1} &= u^k + \alpha(Ax^{k+1} - z^{k+1}). \end{aligned} \quad (20)$$

This method represents a new application of the (heuristic) linearization technique (Ryu & Yin (2022), Section 3.5). In the proof of Proposition 1, we show that (20) corresponds to PAPC/PDFP²O (Chen et al., 2013; Drori et al., 2015) applied to the dual problem (12). Hence, by the relationship of AMA and proximal gradient discussed above, PAPC/PDFP²O can be viewed as a linearized version of proximal gradient. The convergence of (20) can be deduced from that of PAPC/PDFP²O as in Li & Yan (2021).

Proposition 1. *Assume f and g are CCP, and f is μ -strongly convex. Assume that total duality holds and let $(z^{k+1}, x^{k+1}, u^{k+1})$ be the sequence generated in (20). If $0 < \alpha < 2\mu$ and $0 < \alpha\tau\|A\|_2^2 \leq 4/3$, then $(z^{k+1}, x^{k+1}, u^{k+1})$ converge to a saddle point of (11).*

3 Single-block optimization for DPAM

To implement doubly penalized ANOVA regression using backfitting (or block coordinate descent), the subproblem of (6) or (7) with respect to one block while fixing the rest takes the following form (see Section 4 for more details):

$$\min_{\beta} \frac{1}{2n} \|r - X\beta\|_2^2 + \|\Gamma\beta\|_1 + \lambda\|X\beta\|_n, \quad (21)$$

where $\beta \in \mathbb{R}^d$ is the coefficient vector for a specific block, $X \in \mathbb{R}^{n \times d}$ is the basis matrix, $r \in \mathbb{R}^n$ is the residual vector after adjusting for the other blocks, Γ is a diagonal matrix of scaling constants for the HTV/Lasso penalty, and $\lambda \geq 0$ is a tuning parameter for the empirical-norm penalty. For simplicity we omit the subscript of the block index.

In this section, we consider the optimization of (21) where the basis dimension d is of moderate size, but the sample size n can be large. The backfitting algorithm in Yang & Tan (2021) relies on the following result.

Proposition 2 (Yang & Tan (2018)). *Let $\tilde{\beta}$ be a minimizer for the Lasso problem*

$$\min_{\beta} \frac{1}{2n} \|r - X\beta\|_2^2 + \|\Gamma\beta\|_1. \quad (22)$$

If $\|X\tilde{\beta}\|_n = 0$, take $\hat{\beta} = 0$. Otherwise, take $\hat{\beta} = (1 - \lambda/\|X\tilde{\beta}\|_n)_+ \tilde{\beta}$, where $c_+ = c$ for $c \geq 0$ or 0 for $c < 0$. Then $\hat{\beta}$ is a minimizer for problem (21).

Proposition 2 not only makes explicit the different shrinkage effects of the two penalties, HTV and empirical norm, but also provides a direct approach to solving (21): first solving

the Lasso problem (22) and then rescaling (or jointly soft-thresholding) the Lasso solution $\tilde{\beta}$. However, this approach requires determination of the exact Lasso solution and hence can be inefficient in large-scale applications. Soft-thresholding an inexact Lasso solution may not decrease the objective value in problem (21) even when the objective value in (22) is decreased before soft-thresholding. It is also unclear how to derive appropriate stochastic algorithms in this approach for handling large datasets.

We propose and study three first-order methods for directly solving (21) without relying on Proposition 2. Both batch and stochastic algorithms are derived for each method. The first two methods are based on the primal-dual algorithms in Section 2. The third method, called concave conjugate (CC), is derived from a different application of Fenchel duality and can be interpreted as an MM algorithm to tackle the empirical-norm penalty. From our numerical experiments, the CC method performs worse than or similarly as the primal-dual algorithms. For space limitation, the CC method is presented in the Supplement.

In addition to the two-operator splitting methods described in Section 2, it seems natural to consider three-operator splitting methods for solving (21). In Supplement Section I, we present a (tractable) batch algorithm based on the Condat–Vũ algorithm (Condat, 2013; Vũ, 2013). However, its randomization seems to be difficult in our setting.

3.1 Batch primal-dual algorithms

We apply the batch Chambolle–Pock algorithm (16) and linearized AMA (20) to the single-block problem. To make notations more convenient, we rescale problem (21) to

$$\min_{\beta} \frac{1}{2} \|r - X\beta\|_2^2 + n\|\Gamma\beta\|_1 + \lambda\sqrt{n}\|X\beta\|_2, \quad (23)$$

and then formulate problem (23) in the form of (10) as

$$\min_{z, \beta} f(z) + g(\beta), \quad \text{subject to} \quad -z + X\beta = 0, \quad (24)$$

where

$$f(z) = (1/2)\|r - z\|_2^2 + \lambda\sqrt{n}\|z\|_2, \quad (25)$$

for $z \in \mathbb{R}^n$, and $g(\beta) = n\|\Gamma\beta\|_1$ for $\beta \in \mathbb{R}^d$. The dual problem of (24) is $\max_u -f^*(u) - g^*(-X^T u)$, with the associated (full) Lagrangian

$$L(z, \beta; u) = f(z) + g(\beta) + \langle u, X\beta - z \rangle, \quad (26)$$

and the primal-dual Lagrangian

$$L(\beta; u) = g(\beta) + \langle u, X\beta \rangle - f^*(u). \quad (27)$$

Although the choices of f and g are not unique, our choices above are motivated by the fact that both the error term $\|r - X\beta\|_2^2$ and the empirical norm $\|X\beta\|_2$ depend on β only through the linear predictor $X\beta$. Under our formulation (24) of problem (23), the conjugate functions and proximal mappings for f and g can be calculated in a tractable manner. See Section 3.2.1 for a comparison with an alternative formulation.

The conjugate functions f^* and g^* can be calculated in a closed form as

$$f^*(u) = (1/2)(\|u + r\|_2 - \lambda\sqrt{n})_+^2 - (1/2)\|r\|_2^2, \quad (28)$$

for $u \in \mathbb{R}^n$ and $g^*(t) = \sum_{j=1}^d \delta(|t_j| \leq n\Gamma_j)$ for $t \in \mathbb{R}^d$, where Γ_j is the j th diagonal element of Γ , and $\delta_S(x)$ denotes an indicator function for a set S such that $\delta_S(x) = 0$ if $x \in S$, and ∞ otherwise. For scalars $x \in \mathbb{R}$ and $\gamma \geq 0$, denote the soft-thresholding operation as $\mathcal{S}(x, \gamma) = (1 - \gamma/|x|)_+x$. If $x = 0$, then set $\mathcal{S}(x, \gamma) = 0$. For vectors x and r of the same dimensions, we still use $\mathcal{S}(x, r)$ to denote the vector obtained by applying soft-thresholding element-wise, i.e., $\mathcal{S}(x, r) = [(1 - r_i/|x_i|)_+x_i]_i$. For a vector x and a scalar $\gamma \geq 0$, we denote the joint soft-thresholding as $\mathcal{T}(x, \gamma) = (1 - \gamma/\|x\|_2)_+x$. If $x = 0$, then set $\mathcal{T}(x, \gamma) = 0$. The result in Proposition 2 can be stated as $X\hat{\beta} = \mathcal{T}(X\tilde{\beta}, \lambda\sqrt{n})$. With the preceding notation, it can be directly calculated that

$$\mathbf{prox}_{\alpha f}(z) = \frac{\mathcal{T}(z + \alpha r, \alpha\lambda\sqrt{n})}{1 + \alpha}, \quad (29)$$

and $\mathbf{prox}_{\tau g}(\beta) = \mathcal{S}(\beta, \tau n \cdot \text{diag}(\Gamma))$.

Applying the linearized ADMM (15) to problem (24), we obtain

$$z^{k+1} = \mathbf{prox}_{f/\alpha}(X\beta^k + u^k/\alpha) \quad (30a)$$

$$= \mathcal{T}(\alpha X\beta^k + u^k + r, \lambda\sqrt{n})/(1 + \alpha), \quad (30b)$$

$$\beta^{k+1} = \mathbf{prox}_{\tau g/n} \left(\beta^k - \frac{\tau}{n} X^T(u^k + \alpha(X\beta^k - z^{k+1})) \right) \quad (30c)$$

$$= \mathcal{S} \left(\beta^k - \frac{\tau}{n} X^T(u^k + \alpha(X\beta^k - z^{k+1})), \tau \cdot \text{diag}(\Gamma) \right), \quad (30d)$$

$$u^{k+1} = u^k + \alpha(X\beta^{k+1} - z^{k+1}). \quad (30e)$$

Moreover, application of the CP algorithm (16) yields Algorithm 1, where line (31b) follows from (29) and Moreau's identity (8). In fact, Algorithm 1 can be equivalently transformed

Algorithm 1 Single-block Chambolle–Pock

Input Initial values $(\beta^{-1} = \beta^0, u^0)$, number of batch steps B , step sizes τ and α .

for $k = 0, 1, \dots, B - 1$ **do**

$$v^{k+1} = \mathbf{prox}_{\alpha f^*}(v^k + \alpha X(2\beta^k - \beta^{k-1})) \quad (31a)$$

$$= v^k + \alpha X(2\beta^k - \beta^{k-1}) - \frac{\alpha}{1 + \alpha} \mathcal{T}(v^k + \alpha X(2\beta^k - \beta^{k-1}) + r, \lambda\sqrt{n}), \quad (31b)$$

$$\beta^{k+1} = \mathbf{prox}_{\tau g/n}(\beta^k - \frac{\tau}{n} X^T v^{k+1}) \quad (31c)$$

$$= \mathcal{S}\left(\beta^k - \frac{\tau}{n} X^T v^{k+1}, \tau \cdot \text{diag}(\Gamma)\right). \quad (31d)$$

Algorithm 2 Single-block linearized AMA

Input Initial values (β^0, u^0) , number of batch steps B , step sizes τ and α .

for $k = 0, 1, \dots, B - 1$ **do**

$$z^{k+1} = \mathop{\text{argmin}}_z (f(z) - \langle u^k, z \rangle) = \nabla f^*(u^k) \quad (32a)$$

$$= \mathcal{T}(r + u^k, \lambda\sqrt{n}), \quad (32b)$$

$$\beta^{k+1} = \mathbf{prox}_{\tau g/n}\left(\beta^k - \frac{\tau}{n} X^T(u^k + \alpha(X\beta^k - z^{k+1}))\right) \quad (32c)$$

$$= \mathcal{S}\left(\beta^k - \frac{\tau}{n} X^T(u^k + \alpha(X\beta^k - z^{k+1})), \tau \cdot \text{diag}(\Gamma)\right), \quad (32d)$$

$$u^{k+1} = u^k + \alpha(X\beta^{k+1} - z^{k+1}). \quad (32e)$$

from (30) as discussed in Section 2.2. Both algorithms are stated, because we find it somewhat more direct to derive stochastic algorithms from the CP algorithm, whereas the relationship of the CP algorithm with linearized ADMM (30) helps us find a simple criterion to declare a zero solution of β , which is discussed below.

Next, we notice that f in (25) is 1-strongly convex and f^* in (28) is 1-smooth, with the gradient $\nabla f^*(u) = \mathcal{T}(u + r, \lambda\sqrt{n})$. Hence linearized AMA (20) can also be applied to problem (24), leading to Algorithm 2, which differs from (30) only in the z^{k+1} -step.

Convergence results for Algorithms 1 and 2 can be directly obtained from Chambolle & Pock (2011) and Proposition 1 respectively.

Proposition 3. *For Algorithm 1, if $\alpha > 0$, $\tau > 0$ and $\alpha\tau\|X\|_2^2 \leq n$, then (β^k, u^k) converges to a saddle point of (27). For Algorithm 2, if $0 < \alpha < 2$, $\tau > 0$ and $\alpha\tau\|X\|_2^2 \leq 4n/3$, then (z^k, β^k, u^k) converges to a saddle point of (26).*

To conclude this section, we discuss how the sparsity of β can be reached in Algorithms 1 and 2. As shown by Proposition 2, a solution $\hat{\beta}$ to problem (21) may exhibit two types of sparsity. One is element-wise sparsity: $\hat{\beta}$ may be a sparse vector (with some elements being 0), induced by the Lasso penalty $\|\Gamma\beta\|_1$. The other is group sparsity: $\hat{\beta}$ may be an entirely zero vector, as a result of the empirical-norm penalty $\|X\beta\|_n$. For both Algorithms 1 and 2, each iterate β^{k+1} in (31d) or (32d) is obtained using the element-wise soft-thresholding operator \mathcal{S} . On one hand, such β iterates may directly achieve the element-wise sparsity, with some elements being 0. On the other hand, the group sparsity may unlikely be satisfied by any iterate β^{k+1} , because the element-wise soft-thresholding operator \mathcal{S} does not typically produce a zero vector, especially when not all elements of β are penalized (with some diagonal elements of Γ being 0) as in the case of piecewise cross-linear basis functions.

The preceding phenomenon can be attributed to the splitting of the two penalties in (24): $\|\Gamma\beta\|_1$ is assigned to the function g , and $\|X\beta\|_2$ is assigned to the function f through the slack variable $z = X\beta$. From this perspective, a zero solution for β can be more properly detected by checking whether $z^{k+1} = 0$, instead of $\beta^{k+1} = 0$, although the iterates (β^{k+1}, z^{k+1}) converge to $(\hat{\beta}, X\hat{\beta})$, and $\hat{\beta} = 0$ if and only if $X\hat{\beta} = 0$ for X of rank d . In fact, for Algorithm 2, z^{k+1} is determined as (32b) using the joint soft-thresholding operator \mathcal{T} , which may likely produce a zero vector. For Algorithm 1, by the relationship (17b), the corresponding z^{k+1} from (30b) in linearized ADMM can be rewritten in terms of \mathcal{T} as $z^{k+1} = \mathcal{T}(\alpha X(2\beta^k - \beta^{k-1}) + v^k + r, \lambda\sqrt{n})/(1 + \alpha)$. In our implementation, we reset β to 0 after the final iteration if $z^{k+1} = 0$ or equivalently

$$\text{Algorithm 1: } \|\alpha X(2\beta^k - \beta^{k-1}) + v^k + r\|_n \leq \lambda, \quad (33)$$

$$\text{Algorithm 2: } \|r + u^k\|_n \leq \lambda. \quad (34)$$

By this scheme, a zero solution for β can be effectively recovered from Algorithms 1 and 2, even though the β iterates themselves may not yield a zero vector.

3.2 Stochastic primal-dual algorithms

For large datasets (with large n), it is desirable to develop stochastic primal-dual algorithms. Typically, a batch optimization method, such as gradient descent or Algorithms 1 and 2, has a per-iteration cost of $O(nd)$, because the full data matrix (or basis matrix) X needs to be

scanned. Stochastic optimization methods, on the other hand, act only on a single row of X , thus lowering the per-iteration cost to $O(d)$, free of n . A potential advantage of stochastic methods is that their overall efficiency, when measured in the number of batch steps (with each batch step consisting of n iterations) over the full data matrix X , can still be superior over that of batch methods, measured in the number of iterations.

We develop stochastic versions of Algorithms 1 and 2 based on two general principles: replacing the batch gradient with an unbiased or approximately unbiased stochastic gradient for the update of β , and performing randomized coordinate updates for the dual variable u or v . The formal analysis of convergence is left for future work.

3.2.1 Stochastic Chambolle–Pock

As a background, we briefly discuss SPDC (stochastic primal-dual coordinate method) proposed by Zhang & Xiao (2017), as a stochastic version of the CP algorithm (16). The method deals with minimizing an objective function in the form

$$\min_{\beta} \frac{1}{n} \sum_{i=1}^n f_i(X_{i,\cdot}^T, \beta) + \tilde{g}(\beta), \quad (35)$$

where $X_{i,\cdot} \in \mathbb{R}^d$ denotes the transpose of i th row of X , each f_i is convex and smooth, and \tilde{g} is a regularizer (for example, the Lasso penalty) such that its proximal mapping can be easily evaluated. After rescaling by n , (35) can be put in the form of (24), where $f(z) = \sum_{i=1}^n f_i(z_i)$ is coordinate-wise separable with $z = (z_1, \dots, z_n)^T$ and $g(\beta) = n\tilde{g}(\beta)$. Consequently, the conjugate of f is separable: $f^*(v) = \sum_{i=1}^n f_i^*(v_i)$, where $v = (v_1, \dots, v_n)^T$ and f_i^* is the conjugate of f_i . The dual update in the CP algorithm (16) also becomes separable: the i th element, v_i^{k+1} , of v^{k+1} in (16a) can be obtained as

$$v_i^{k+1} = \mathbf{prox}_{\alpha f_i^*}(v_i^k + \alpha X_{i,\cdot}^T(2\beta^k - \beta^{k-1})). \quad (36)$$

In other words, each element v_i^{k+1} can be updated with cost $O(d)$, independently of the other elements in v^{k+1} . Such separability is exploited by SPDC to achieve two properties of unbiasedness, given the history up to (v^k, β^k) . First, one coordinate of v^k (for example i th) is randomly selected and then updated to v_i^{k+1} , the i th element in the full update v^{k+1} in (36). The resulting update of v , different from v^k by one coordinate, is unbiased for the full update v^{k+1} . Second, a stochastic gradient, G^{k+1} , is created to replace the batch gradient

$X^\top v^{k+1}/n$ in the update β^{k+1} in (16b), such that G^{k+1} is unbiased for $X^\top v^{k+1}/n$ with the full update v^{k+1} . The choice of G^{k+1} in SPDC is defined as $G^{k+1} = X_{i,\cdot}(v_i^{k+1} - v_i^k) + \frac{1}{n}X^\top v^k$, corresponding to the SAGA method (Defazio et al., 2014) discussed below.

Our problem (21) can be put in the form of (35), with $f_i(t_i) = (y_i - t_i)^2/2$ and $\tilde{g}(\beta) = \|\Gamma\beta\|_1 + \lambda\|X\beta\|_n$, for which the proximal mapping is difficult to evaluate. Hence our problem does not fit into the setting of SPDC. Moreover, our formulation (24) of problem (21) differs substantially from (35) in that the function f in (25) is not separable due to the inclusion of the empirical norm. In our CP algorithm (Algorithm 1), evaluating one coordinate of v^{k+1} in (31b) is as difficult as evaluating the full v^{k+1} , costing $O(nd)$. Therefore, we need to generalize related ideas in SPDC to derive a stochastic CP algorithm with non-separable f .

To approximate the batch update v^{k+1} , we apply randomized coordinate minimization, i.e., evaluating the proximal mapping in (31a) for a randomly selected coordinate while fixing the remaining coordinates. This operation is distinct from that of evaluating one randomly selected coordinate of the full update v^{k+1} , although the two operations coincide in the special case of separable f as in SPDC. We show that the coordinate minimization can be done with cost $O(d)$ provided we additionally maintain $\|v^k + r\|_2^2$.

Proposition 4. *For $b \in \mathbb{R}^n$ and $\alpha \geq 0$, let*

$$\mathbf{prox}_{\alpha f^*}(b, i, v_{-i}^k) = \operatorname{argmin}_{v_i} \frac{1}{2}\|v - b\|_2^2 + \alpha f^*(v), \quad (37)$$

where f^* is defined in (28), and v_i is the i th coordinate of v , while the remaining coordinates of v are fixed at $v_{-i}^k = (v_1^k, \dots, v_{i-1}^k, v_{i+1}^k, \dots, v_n^k)$. Then $\mathbf{prox}_{\alpha f^*}(b, i, v_{-i}^k) = -r_i$ if $b_i + r_i = 0$; otherwise $\mathbf{prox}_{\alpha f^*}(b, i, v_{-i}^k) = c(b_i + r_i) - r_i$, with

$$c = \begin{cases} 1, & \text{if } (b_i + r_i)^2 + \|v^k + r\|_{-i}^2 \leq n\lambda^2, \\ \left(1 + \frac{\alpha\lambda\sqrt{n}}{|b_i + r_i|}\right) / (1 + \alpha), & \text{if } \|v^k + r\|_{-i}^2 = 0 \text{ and } |b_i + r_i| > \lambda\sqrt{n}, \\ c^*, & \text{otherwise,} \end{cases}$$

where $\|v^k + r\|_{-i}^2 = \|v^k + r\|_2^2 - (v_i^k + r_i)^2$ and c^* is the root of equation

$$\left(1 + \alpha - \frac{\alpha\lambda\sqrt{n}}{\sqrt{c^2(b_i + r_i)^2 + \|v^k + r\|_{-i}^2}}\right) c = 1.$$

Such c^* uniquely lies in $(0, 1)$.

Given the history up to (v^k, β^k) , we randomly select one coordinate (for example i th) and define the stochastic update v^{k+1} as follows:

$$v_i^{k+1} = \mathbf{prox}_{\alpha f^*}(v^k + \alpha X^T(2\beta^k - \beta^{k-1}), i, v_{-i}^k) \quad \text{or} \quad v_l^{k+1} = v_l^k \text{ for } l \neq i, \quad (38)$$

while keeping the remaining elements as in v^k . Note that v^{k+1} here differs from the batch update v^{k+1} in (31a), which will henceforth be denoted as v_B^{k+1} . From Proposition 4, we observe that the coordinate proximal mapping (37) costs $O(1)$ to compute, once b_i and $\|v^k + r\|_{-i}^2$ are determined. For our Algorithm 3, the former is evaluated as $v_i^k + \alpha X_{i,\cdot}^T(2\beta^k - \beta^{k-1})$ with cost $O(d)$, and the latter costs $O(1)$ to compute as we maintain $\|v^k + r\|_2^2$. Therefore, the proposed update v^{k+1} can be computed with cost $O(d)$.

For the primal update β^{k+1} , the general idea is to replace the batch gradient $G_B^{k+1} = X^T v_B^{k+1}/n$ by a stochastic approximation G^{k+1} , and define

$$\beta^{k+1} = \mathbf{prox}_{\tau g/n}(\beta^k - \tau G^{k+1}) = \mathcal{S}(\beta^k - \tau G^{k+1}, \tau \cdot \text{diag}(\Gamma)), \quad (39)$$

where v_B^{k+1} denotes the batch update v^{k+1} in (31a), to be distinguished from the partial update v^{k+1} defined above. There are at least three choices for G^{k+1} , corresponding to three related stochastic gradient methods. Given the approximation v_i^{k+1} , the first is the standard stochastic gradient method (SG) (Bottou et al., 2018): $G^{k+1} = X_{i,\cdot} v_i^{k+1}$. The second is based on the stochastic average gradient (SAG) method (Roux et al., 2012):

$$G^{k+1} = \frac{1}{n} X_{i,\cdot} (v_i^{k+1} - v_i^k) + \frac{1}{n} \sum_{i=1}^n X_{i,\cdot} v_i^k = \frac{1}{n} X_{i,\cdot} (v_i^{k+1} - v_i^k) + \underbrace{\frac{1}{n} X^T v^k}_{w^k}. \quad (40)$$

The third is based on SAGA (Defazio et al., 2014):

$$G^{k+1} = X_{i,\cdot} (v_i^{k+1} - v_i^k) + \frac{1}{n} \sum_{i=1}^n X_{i,\cdot} v_i^k = X_{i,\cdot} (v_i^{k+1} - v_i^k) + \underbrace{\frac{1}{n} X^T v^k}_{w^k}. \quad (41)$$

For (40) and (41), the variable w^k can be updated as $w^{k+1} = w^k + X_{i,\cdot} (v_i^{k+1} - v_i^k)/n$, so that there is no need to re-calculate the average in each iteration.

There is an extensive literature on the three methods and other variants in the standard setting (35) or similar ones. Both SAG and SAGA are designed for variance reduction, and SAG often yields smaller variance than SAGA. Moreover, given the history, the stochastic gradients in SG and SAGA are known to be unbiased, but that in SAG is biased, in standard

Algorithm 3 Stochastic Chambolle–Pock

Input Initial (β^0, v^0) , number of batch steps B , step sizes α and τ .

Initialize $w^0 = X^\top v^0/n$, and $L^2 = \|v^0 + r\|_2^2$.

for $k = 0, 1, \dots, nB - 1$ **do**

Pick i uniformly from $\{1, \dots, n\}$, and perform the following updates:

$$v^{k+1}, G^{k+1}, \text{ and } \beta^{k+1} \text{ by (38) with } L^2 = \|v^k + r\|_2^2, (41), \text{ and (39),}$$

$$w^{k+1} = w^k + X_{i,\cdot}(v_i^{k+1} - v_i^k)/n,$$

$$L^2 \leftarrow L^2 - (v_i^k + r_i)^2 + (v_i^{k+1} + r_i)^2.$$

settings. Following SPDC, we adopt (41) based on SAGA as the stochastic gradient in our update of β . The resulting algorithm is summarized in Algorithm 3.

Convergence analysis of the proposed stochastic algorithm remains to be studied. As discussed earlier in this section, due to separable f in problem (35), the closely related SPDC method enjoys two properties of (exact) unbiasedness for the updates of v and β , when compared with the corresponding batch CP algorithm. Such a simple relationship no longer holds between the stochastic Algorithm 3 and batch Algorithm 1 in our setting, due to non-separable f . Given up to k th iteration, our stochastic update v^{k+1} or gradient G^{k+1} is not exactly unbiased for the batch version v_B^{k+1} or G_B^{k+1} , because randomized coordinate minimization is used instead of evaluating a randomly selected coordinate of the batch update v_B^{k+1} (which is as costly as evaluating v_B^{k+1} itself with non-separable f). Further study is needed to tackle these complications for theoretical analysis.

3.2.2 Stochastic linearized AMA

We develop a stochastic version of our linearized AMA algorithm (Algorithm 2). For technical convenience, we reorder Algorithm 2 such that the dual variable is updated first, and the primal update is moved to the end of each iteration, i.e.,

$$u^{k+1} = u^k + \alpha(X\beta^k - \nabla f^*(u^k)) \quad (42a)$$

$$\beta^{k+1} = \mathbf{prox}_{\tau g/n} \left[\beta^k - \frac{\tau}{n} X^\top (u^{k+1} + \alpha(X\beta^k - \nabla f^*(u^{k+1}))) \right]. \quad (42b)$$

Note that the auxiliary variable $z^k = \nabla f^*(u^k)$ and $z^{k+1} = \nabla f^*(u^{k+1})$ are absorbed in the preceding updates such that only primal and dual variables are left.

To approximate the dual update (42a), it is desirable to perform a randomized coordinate update as follows. We randomly select one coordinate (for example i th) and define the stochastic update u^{k+1} as follows:

$$u_i^{k+1} = u_i^k + \alpha(X_{i,\cdot}^\top \beta^k - \nabla_i f^*(u^k)) \quad \text{or} \quad u_l^{k+1} = u_l^k \text{ for } l \neq i, \quad (43)$$

where $\nabla_i f^*(u^k)$ denotes the i th element of $\nabla f^*(u^k)$, i.e., $\partial f^*(u^k)/\partial u_i$. Note that u^{k+1} here differs from the batch update u^{k+1} in (42a), which will henceforth be denoted as u_B^{k+1} . While evaluating $X_{i,\cdot}^\top \beta^k$ costs $O(d)$, evaluating one coordinate of $\nabla f^*(u)$ may in general cost $O(n)$ for non-separable f . However, unlike stochastic Chambolle–Pock in Section 3.2.1 where coordinate minimization is employed to handle the non-separability, evaluating $\nabla_i f^*(u^k)$ turns out to cost only $O(1)$ in the current setting, due to the special form of f^* . In fact, by the definition of f^* in (28), $\nabla f^*(u^k)$ takes the form of joint soft-thresholding:

$$\nabla f^*(u^k) = \mathcal{T}(r + u^k, \lambda\sqrt{n}) = \left(1 - \frac{\lambda\sqrt{n}}{\|r + u^k\|_2}\right)_+ \cdot (r + u^k).$$

To evaluate $\nabla_i f^*(u^k)$, it suffices to compute the scalar factor above, which costs $O(1)$ if we additionally maintain $\|r + u^k\|_2$ as shown in Algorithm 4. Therefore, the proposed update u^{k+1} can be computed with cost $O(d)$.

To approximate the primal update (42b), the general strategy is to construct a stochastic estimate G^{k+1} for the batch gradient

$$G_B^{k+1} = \frac{1}{n} X^\top u_B^{k+1} + \frac{\alpha}{n} X^\top (X \beta^k - \nabla f^*(u_B^{k+1})), \quad (44)$$

where u_B^{k+1} denotes the batch update u^{k+1} in (42a), to be distinguished from the partial update u^{k+1} defined above (which differs from u^k by one coordinate). Note that (44) is more complicated than the batch gradient $X^\top u_B^{k+1}/n$ in the CP algorithm. The additional second term involves $\nabla f^*(u_B^{k+1})$, which depends on the unknown full update u_B^{k+1} in a nonlinear manner. To proceed, the only feasible approach seems to be replacing the batch update u_B^{k+1} by the partial update u^{k+1} and approximating the second term by $\alpha(X_{i,\cdot}^\top \beta^k - \nabla_i f^*(u^{k+1})) \cdot X_{i,\cdot}$. For the first term in (44), in line with the approximation of the second term, it is natural to also replace the batch update u_B^{k+1} by the partial update u^{k+1} . Combining the preceding choices leads to the stochastic gradient

$$G^{k+1} = w^k + \frac{1}{n} X_{i,\cdot} (u_i^{k+1} - u_i^k) + \alpha X_{i,\cdot} (X_{i,\cdot}^\top \beta^k - \nabla_i f^*(u^{k+1})), \quad (45)$$

where u^{k+1} is the partial update defined in (43), and $w^k = X^\top u^k/n$ can be updated as $w^{k+1} = w^k + X_{i,\cdot}(u_i^{k+1} - u_i^k)/n$. The primal update of β is then defined as

$$\beta^{k+1} = \mathbf{prox}_{\tau g/n}(\beta^k - \tau G^{k+1}) = \mathcal{S}(\beta^k - \tau G^{k+1}, \tau \cdot \text{diag}(\Gamma)), \quad (46)$$

The resulting algorithm is summarized in Algorithm 4. The stochastic gradient G^{k+1} above can be seen to be in spirit of SAG. Alternatively, SAGA can also be employed to approximate the first term in (44). The corresponding stochastic gradient is

$$G^{k+1} = w^k + X_{i,\cdot}(u_i^{k+1} - u_i^k) + \alpha X_{i,\cdot}(X_{i,\cdot}^\top \beta^k - \nabla_i f^*(u^{k+1})), \quad (47)$$

which leads to the SAGA option in Algorithm 4.

Convergence analysis of Algorithm 4 remains to be studied, although with slightly different complications than in Algorithm 3. Given up to k th iteration, the stochastic update u^{k+1} is unbiased for the batch update u_B^{k+1} in spite of non-separable f in our problem. However, the stochastic gradient G^{k+1} is not exactly unbiased for the batch gradient G_B^{k+1} , due to the nonlinear dependency of $\nabla f^*(u_B^{k+1})$ on u_B^{k+1} as discussed earlier.

Algorithm 4 Single-block stochastic linearized AMA

Input Initial (β^0, u^0) , number of batch steps B , step sizes α and τ .

Initialize $w^0 = X^\top u^0/n$, and $L^2 = \|u^0 + r\|_2^2$.

for $k = 0, 1, \dots, nB - 1$ **do**

Pick i uniformly from $\{1, \dots, n\}$, and perform the following updates:

$$u^{k+1} \text{ by (43) with } \nabla_i f^*(u^k) = (1 - \lambda\sqrt{n}/L)_+ \cdot (r_i + u_i^k),$$

$$L^2 \leftarrow L^2 - (r_i + u_i^k)^2 + (r_i + u_i^{k+1})^2,$$

$$\nabla_i f^*(u^{k+1}) = (1 - \lambda\sqrt{n}/L)_+ \cdot (r_i + u_i^{k+1}),$$

if AMA-SAG **then**

$$G^{k+1} \text{ and } \beta^{k+1} \text{ by (45) and (46),}$$

if AMA-SAGA **then**

$$G^{k+1} \text{ and } \beta^{k+1} \text{ by (47) and (46),}$$

$$w^{k+1} = w^k + X_{i,\cdot}(u_i^{k+1} - u_i^k)/n.$$

4 Multi-block optimization for DPAM

4.1 Training and predictions

We use the backfitting algorithm in Yang & Tan (2018, 2021) to solve the multi-block problems (6) and (7). For completeness, we briefly introduce the method here. The top-level idea is updating one selected block while fixing the rest and then cycling over all blocks. To solve the single-block problem, methods in Section 3 can be used.

Let $\Psi_{S_k}^\dagger$ be the basis matrix formed from the basis vector Ψ_{S_k} , i.e., the i th row of $\Psi_{S_k}^\dagger$ is the transpose of $\Psi_{S_k}(X_i)$ for $i = 1, \dots, n$. For the linear regression problem (6), to avoid interference between β_0 and other coefficients, we solve a slightly modified problem

$$\min_{(\beta_{S_k})_{k,S_k}} \frac{1}{2} \left\| \tilde{Y} - \sum_{k,S_k} \tilde{\Psi}_{S_k}^\dagger \beta_{S_k} \right\|_n^2 + \sum_{k,S_k} \left(\|\Gamma_{S_k} \beta_{S_k}\|_1 + \lambda_k \|\tilde{\Psi}_{S_k}^\dagger \beta_{S_k}\|_n \right), \quad (48)$$

where $\tilde{Y} = Y - \bar{Y}$ and $\tilde{\Psi}_{S_k}^\dagger = \Psi_{S_k}^\dagger - \bar{\Psi}_{S_k}^\dagger$ are empirically centered versions of Y and $\Psi_{S_k}^\dagger$. See Yang & Tan (2021), Section 3.3, for a formal justification, which shows that the modified problem is equivalent to the original problem (6) with an intercept introduced within each block in addition to β_0 . For backfitting, the subproblem of (48) with respect to the block β_{S_k} while fixing the rest at the current estimates $(\hat{\beta}_{S_j})_{j,S_j}$ is

$$\min_{\beta_{S_k}} \frac{1}{2n} \|r - \tilde{\Psi}_{S_k}^\dagger \beta_{S_k}\|_n^2 + \|\Gamma_{S_k} \beta_{S_k}\|_1 + \lambda_k \|\tilde{\Psi}_{S_k}^\dagger \beta_{S_k}\|_n,$$

where $r = Y - \sum_{S_j \neq S_k} \tilde{\Psi}_{S_j}^\dagger \hat{\beta}_{S_j}$. This is in the form of the single-block problem studied in Section 3, with $X = \tilde{\Psi}_{S_k}^\dagger$, $\beta = \beta_{S_k}$, and $\Gamma = \Gamma_{S_k}$.

For the prediction given new data matrix X^{new} , we construct the basis matrices $(\Psi_{S_k}^{\text{new}})_{k,S_k}$ accordingly (for example, using marginal knots fixed at univariate quantiles from the training data). Then the predicted response vector is $Y^{\text{pred}} = \bar{Y} + \sum_{k,S_k} (\Psi_{S_k}^{\text{new}} - \bar{\Psi}_{S_k}^\dagger) \hat{\beta}_{S_k}$. Note that \bar{Y} and $\bar{\Psi}_{S_k}^\dagger$ are the means of the training data.

For the logistic regression problem (7), we keep the original response vector and the overall intercept β_0 and solve the modified problem:

$$\min_{\beta_0, (\beta_{S_k})_{k,S_k}} \frac{1}{n} \sum_{i=1}^n l(Y_i, f_i) + \sum_{k,S_k} \left(\|\Gamma_{S_k} \beta_{S_k}\|_1 + \lambda_k \|\tilde{\Psi}_{S_k}^\dagger \beta_{S_k}\|_n \right),$$

where $f = (f_1, \dots, f_n)^\top = \beta_0 + \sum_{k,S_k} \tilde{\Psi}_{S_k}^\dagger \beta_{S_k}$ and $\tilde{\Psi}_{S_k}^\dagger$ are empirically centered basis matrices. For training, we replace the logistic loss by its second order Taylor expansion at the current

estimates $\hat{\beta}_0$ and $(\hat{\beta}_{S_k})_{k,S_k}$, and further replace the Hessian matrix $H = \hat{p}(1-\hat{p})$ by a constant upper bound $1/4$ to obtain a majorization of the logistic loss. For backfitting, the objective in the sub-problem with respect to β_0 and β_{S_k} reduces to

$$\min_{\beta_0, \beta_{S_k}} \frac{1}{2n} \|r - \beta_0 - \tilde{\Psi}_{S_k}^\dagger \beta_{S_k}\|_2^2 + 4\|\Gamma_{S_k} \beta_{S_k}\|_1 + 4\lambda_k \|\tilde{\Psi}_{S_k}^\dagger \beta_{S_k}\|_n,$$

where $r = \hat{\beta}_0 + \tilde{\Psi}_{S_k}^\dagger \hat{\beta}_{S_k} + 4(Y - \hat{p})$, $\hat{p} = 1/(1 + \exp(-\hat{f}))$ and $\hat{f} = \hat{\beta}_0 + \sum_{j,S_j} \Psi_{S_j}^\dagger \hat{\beta}_{S_j}$. Then the intercept can be directly updated as the mean of r , denoted as \bar{r} . The sub-problem with respect to only β_{S_k} becomes

$$\min_{\beta_{S_k}} \frac{1}{2n} \|\tilde{r} - \tilde{\Psi}_{S_k}^\dagger \beta_{S_k}\|_2^2 + 4\|\Gamma_{S_k} \beta_{S_k}\|_1 + 4\lambda_k \|\tilde{\Psi}_{S_k}^\dagger \beta_{S_k}\|_n,$$

where $\tilde{r} = r - \bar{r}$. This is the standard form of single-block optimization in Section 3.

For the prediction or classification given new data matrices X^{new} , we construct the basis matrices $(\Psi_{S_k}^{\text{new}})_{k,S_k}$ similarly as in the linear modeling. Then the predicted f is $f^{\text{pred}} = \hat{\beta}_0 + \sum_{k,S_k} (\Psi_{S_k}^{\text{new}} - \tilde{\Psi}_{S_k}^\dagger) \hat{\beta}_{S_k}$, and the predicted probability is $p^{\text{pred}} = 1/(1 + \exp(-f^{\text{pred}}))$.

4.2 Comparison with AS-BDT

In Yang & Tan (2018, 2021), the single-block problem is solved by first solving the Lasso problem (22) using an active-set descent algorithm (Osborne et al., 2000) and then jointly soft-thresholding the Lasso solution. The resulting backfitting algorithm is called AS-BDT (active-set block descent and thresholding). As the active-set algorithm is efficient for solving sparse Lasso problems, AS-BDT tends to perform well if the average size of nonzero coefficients per block (corresponding to active basis functions) is small. Moreover, the active-set information, including the signs of nonzero coefficients and the associated Cholesky decompositions, can be passed from the previous cycle to speed up the active-set algorithm within each block and hence achieve computational savings for AS-BDT. However, AS-BDT may not be suitable for handling large datasets, especially with non-sparse blocks.

Compared with AS-BDT, the proposed methods (particularly stochastic primal-dual algorithms) are more adaptive to large-sample scenarios. They are expected to achieve near optimal objective values at relatively lower costs. On the other hand, the primal-dual algorithms are not designed to take advantage of structural information from the previous cycle of backfitting to achieve acceleration as in AS-BDT.

To exploit gains from different methods, a hybrid algorithm can be considered by combining stochastic primal-dual and the active-set algorithms sequentially. At the beginning of backfitting, stochastic primal-dual algorithms can be used to obtain a decent decrease of the training loss. Then the active-set method can be used to fine-tune the solutions if necessary. Alternatively, acceleration can also be achieved by cycling over a subset of nonzero blocks and adjusting the subset iteratively, as discussed in Radchenko & James (2010). Our numerical experiments are focused on the direct implementation of AS-BDT and the proposed methods. We leave investigation of hybrid methods to future work.

5 Numerical experiments

We conduct numerical experiments to evaluate various algorithms for training DPAMs. We first consider the single-block optimization and then move on to the multi-block linear and logistic regressions, with both simulated data and real data.

5.1 Single-block experiments

Consider the following regression function, motivated from Lin & Zhang (2006), Section 7, but with more complex nonlinear interactions:

$$\begin{aligned}
 f(x) = & \left(\sum_{i=1}^7 \tilde{g}_i(x_i) \right) + \tilde{g}_1(x_3x_4) + \tilde{g}_2\left(\frac{x_1+x_3}{2}\right) + \tilde{g}_3(x_1x_2) \\
 & + \tilde{g}_4(x_4x_5) + \tilde{g}_5\left(\frac{x_4+x_6}{2}\right) + \tilde{g}_6\left(\frac{x_5+x_2}{2}\right) + \tilde{g}_7(x_6x_7),
 \end{aligned} \tag{49}$$

where $\{g_i, i = 1, \dots, 7\}$ are functions defined on the interval $[0, 1]$ as

$$\begin{aligned}
 g_1(x) &= x, & g_2(x) &= (2x-1)^2, & g_3(x) &= \frac{1}{1+x}, \\
 g_4(x) &= 0.1 \sin(2\pi x) + 0.2 \cos(2\pi x) + 0.3 \sin^2(2\pi x) + 0.4 \cos^3(2\pi x) + 0.5 \sin^3(2\pi x), \\
 g_5(x) &= \frac{\sin(2\pi x)}{2 - \sin(2\pi x)}, & g_6(x) &= \frac{\sin(4\pi x)}{2 + \sin(2\pi x)}, & g_7(x) &= \frac{\cos(4\pi x)}{2 + \cos(2\pi x)},
 \end{aligned}$$

and $\{\tilde{g}_i, i = 1, \dots, 7\}$ are centered versions $\{\tilde{g}_i(x) = g_i(x) - \int_0^1 g_i(x) dx\}$. The inputs $X_i = (X_{i,1}, \dots, X_{i,7})$ for $i = 1, \dots, n$ are i.i.d. uniformly distributed on $[0, 1]^7$. A normal noise with standard deviation 0.5138 is added to give a signal-to-noise ratio of 3:1. That is, the response variables $\{Y_1, \dots, Y_n\}$ are generated by $Y_i = f(X_i) + \epsilon_i$ where $\epsilon_i \sim N(0, 0.5138^2)$.

We consider the linear DPAM (6) for Y on X with differentiation order $m = 2$ (i.e., piecewise cross-linear basis functions), the marginalization H being the average operator on the training set (which are used in all our experiments), and 11 marginal knots defined as the quantiles by 10% in the training set for each covariate (resulting in 10 univariate basis functions for each covariate). In particular, we consider the subproblem of fitting Y on the basis matrix $\Psi_{4,5}^\dagger$, associated with two-way interactions from x_4 and x_5 :

$$\min_{\beta_{4,5}} \frac{1}{2n} \|\tilde{Y} - \tilde{\Psi}_{4,5}^\dagger \beta_{4,5}\|_2^2 + \|\Gamma_{4,5} \beta_{4,5}\|_1 + \lambda \|\tilde{\Psi}_{4,5}^\dagger \beta_{4,5}\|_n, \quad (50)$$

where \tilde{Y} and $\tilde{\Psi}_{4,5}^\dagger$ are empirically centered versions of Y and $\Psi_{4,5}^\dagger$ respectively. Based on Yang & Tan (2021), $\Gamma_{4,5} = \rho \cdot \text{diag}(0, 1, \dots, 1)$ is defined to represent the HTV/Lasso penalty with differentiation order $m = 2$. The basis matrix $\tilde{\Psi}_{4,5}^\dagger$ includes $10^2 = 100$ basis functions and $\beta_{4,5} \in \mathbb{R}^{100}$. Focusing on the large-scale problem, we take $n = 50000$.

We design experiments with different ρ and λ to evaluate our algorithms, using Proposition 2. For any ρ , we first compute $\tilde{\beta}_{4,5}(\rho)$ as a solution to the Lasso problem, with the empirical-norm penalty removed from (50). Let $\lambda_0(\rho) = \|\tilde{\Psi}_{4,5}^\dagger \tilde{\beta}_{4,5}\|_n$. Then for any $\lambda \geq \lambda_0(\rho)$, a solution $\hat{\beta}_{4,5}$ to problem (50) is 0. For $\lambda < \lambda_0(\rho)$, a solution $\hat{\beta}_{4,5}$ can be obtained by jointly shrinking $\tilde{\beta}_{4,5}(\rho)$. We let ρ vary in $\{2^{-15}, 2^{-18}, 2^{-21}\}$, and for each ρ , we take λ to be either $\lambda_0(\rho)/4$ or $2\lambda_0(\rho)$, corresponding to a nonzero or completely zero solution $\hat{\beta}_{4,5}$. As ρ decreases in $\{2^{-15}, 2^{-18}, 2^{-21}\}$, the number of nonzero scalar coefficients in the Lasso solution $\tilde{\beta}_{4,5}$ increases from 20 to 37 and further to 62 out of 100.

In the single-block experiments, we compare the following algorithms. The AS-BDT algorithm in Yang & Tan (2018) is used to compute exact solutions.

- **Batch algorithms**

- **CP:** The Chambolle–Pock algorithm (Algorithm 1).
- **AMA:** The linearized AMA (Algorithm 2).
- **CC:** The Concave conjugate algorithm with perturbation (Algorithm S1 in the Supplement). Choose $\delta = 10^{-6}$.

- **Stochastic algorithms**

- **Stoc-CP:** Algorithm 3. Each step operates on a single row of $\tilde{\Psi}_{4,5}^\dagger$. Therefore we

count n consecutive steps as one batch step. Each step needs to solve a non-linear univariate equation on a fixed interval $(0, 1)$.

- **Stoc-AMA-SAG and Stoc-AMA-SAGA:** Algorithm 4. Similarly as in Stoc-CP, we count n steps as one batch step.
- **Stoc-CC:** Algorithm S2 in the Supplement. One outer iteration with cost $O(nd)$ is counted as one batch step.

Step sizes for batch and stochastic algorithms are tuned manually, as would be done in practice. See Supplement Section VI.1 for detailed information. The algorithms are evaluated by their performances in reducing the optimality gap where the optimal objective value is computed from AS-BDT. The results are shown in Figure 1. All algorithms start from an initial $\beta^0 = 0$, and primal-dual algorithms additionally set the initial dual variable as $u^0 = \tilde{\Psi}_{4,5}^\dagger \beta^0 - \tilde{Y} = -\tilde{Y}$. For the stochastic algorithms, we plot the mean performance as well as the minimum and maximum optimality gaps across 10 repeated runs with different random seeds. We observe several trends across the experiments:

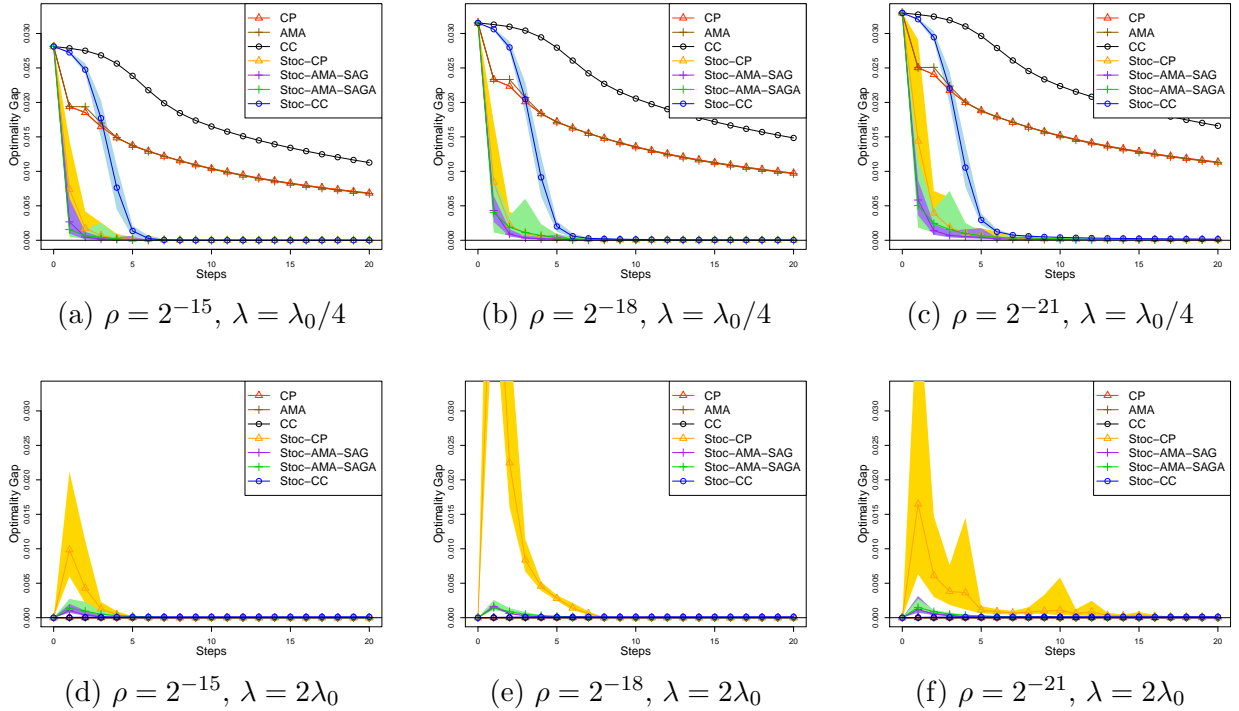


Figure 1: Single-block experiments with varying ρ and λ . The 0 gap is indicated by the black solid line.

- **Effect of λ :** When $\lambda = \lambda_0/4$, the initial value $\beta^0 = 0$ is sub-optimal, and all algorithms exhibit a decreasing pattern. When $\lambda = 2\lambda_0$, the initial value $\beta^0 = 0$ is optimal. In this case, all stochastic primal-dual algorithms follow a non-monotone pattern, whereas the batch primal-dual algorithms stay close to 0 because after tuning, nearly optimal step sizes (τ close to 0 and large α) are applied.
- **Effect of ρ :** With $\lambda = \lambda_0/4$ fixed, as ρ decreases from 2^{-15} to 2^{-18} and further to 2^{-21} , while the exact solution becomes denser, both the batch and stochastic algorithms remain relatively stable in their performances.
- **Batch vs Stochastic:** All stochastic algorithms are substantially faster than their deterministic counterparts in the case of $\lambda = \lambda_0/4$.
- **CP vs AMA:** CP and AMA, batch and stochastic versions, lead to similar performances when $\lambda = \lambda_0/4$, although they are derived in technically different manners.
- **Primal-dual vs CC:** When $\lambda = \lambda_0/4$, the primal-dual algorithms, batch and stochastic versions, perform better than CC. When $\lambda = 2\lambda_0$ and the initial $\beta^0 = 0$ is optimal, CC benefits from the monotonicity, albeit in terms of the perturbed objective.

5.2 Multi-block experiments

We compare several algorithms for training multi-block DPAMs (Yang & Tan, 2018, 2021), in two experiments for linear regression (6) on simulated data and two experiments for logistic regression (7) on both simulated and real data. The experiment for linear regression using the phase shift model (Friedman, 1991) is presented in the Supplement, where DPAM with up to three-way interactions (as well as two-way interactions) is trained. Throughout, we use constant penalty parameters ρ and λ for the HTV/Lasso and empirical-norm penalties.

We evaluate the algorithms in terms of their performances in decreasing the training loss after the same number of epochs over data and basis blocks. Because the size d_{S_k} of a block S_k varies from block to block, we count one *cycle* over all blocks, with one *scan* of the full dataset in each block, as one single *epoch*. Specifically, if an algorithm scans the full dataset for T times within the block S_k , the corresponding number of epochs is counted as $Td_{S_k}/\sum_{S_l} d_{S_l}$. All algorithms start from an initial value 0 within each block.

- **Batch algorithms**

- **AS-BDT:** In each block, one scan is counted when the active set is adjusted (enlarged or reduced) or when the final active set is identified. The number of scans may vary from block to block, depending on the sparsity of the solution.
- **CC, CP and AMA:** Each batch step is counted as one scan. For simplicity, a fixed number, 6, of batch steps, are performed across all blocks in each backfitting cycle. For all primal-dual algorithms (including their stochastic versions), the coefficients are reset to 0 using conditions (33) and (34) within each block, to promote sparsity and improve performances.

- **Stochastic algorithms**

- **Stoc-CC, Stoc-CP and Stoc-AMA-SAG:** One batch step which consists of n consecutive steps is defined as one scan, as in the single-block experiment. The same number of batch steps is fixed across all blocks, either 3 for linear regression or 5 for logistic regression. For Stoc-CC (as well as CC), only one majorization ($B = 1$) is performed within each block.

Step sizes are tuned manually; see detailed information in Supplement Section VI.2.

5.2.1 Synthetic linear regression

For $n = 50000$, we generate $X_i = (X_{i,1}, X_{i,2}, \dots, X_{i,10})$ uniformly on $[0, 1]^{10}$ and $Y_i = f(X_i) + \epsilon_i$, $i = 1, \dots, n$, where $\epsilon_i \sim N(0, 0.5138^2)$ and f is defined as (49). Note that X_8 , X_9 and X_{10} are spurious variables. We apply the linear DPAM (6), with differentiation order $m = 2$ (i.e., piecewise cross-linear basis functions), interaction order $K = 2$ (main effects and two-way interactions), and 6 marginal knots from data quantiles by 20% (5 basis functions for each main effect). The performances of various algorithms are reported in Figure 2, under different choices of $\rho \in \{2^{-16}, 2^{-19}, 2^{-22}\}$ and $\lambda \in \{\|\tilde{Y}\|_n/2^6, \|\tilde{Y}\|_n/2^8, \|\tilde{Y}\|_n/2^{10}\}$, where \tilde{Y} is the centered version of Y . These penalty parameters ρ and λ are chosen, to demonstrate a range of sparsity levels and mean squared errors (MSEs) calculated on a validation set. For solutions from AS-BDT (after convergence declared), the sparsity levels and MSEs under different tuning parameters are summarized in Table 1. The sparsity levels from stochastic

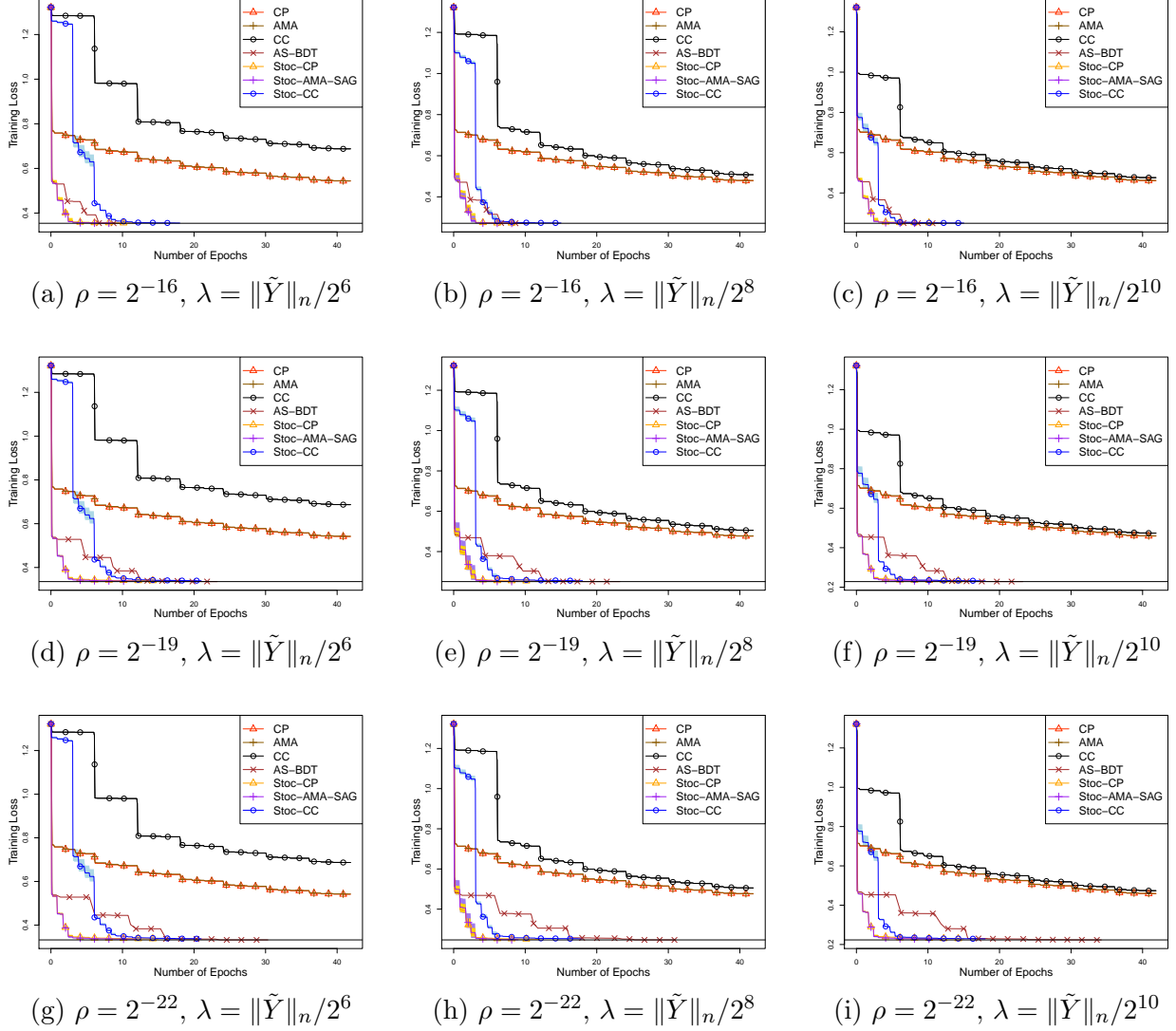


Figure 2: DPAM training in synthetic linear regression. The minimal training loss achieved from AS-BDT is given by the black solid line. For the stochastic algorithms, we plot the mean as well as the minimum and maximum training losses across 10 repeated runs.

primal-dual algorithms are reported in Supplement Table S2. A tolerance of 10^{-3} in the objective value is checked after each cycle over all blocks to declare convergence.

5.2.2 Synthetic logistic regression

The logistic regression model is extended from the linear regression model in Section 5.2.1. For $n = 50000$, we generate $X_i = (X_{i,1}, X_{i,2}, \dots, X_{i,10})$ uniform on $[0, 1]^{10}$ and Y_i as Bernoulli with success probability $\text{expit}(f(X_i))$, $i = 1, \dots, n$, where $\text{expit}(f) = 1/(1 + \exp(-f))$, and

Table 1: Sparsity and MSEs for synthetic linear regression.

$\log_2(\rho^{-1})$	16			19			22		
$\log_2(\lambda^{-1})$	6	8	10	6	8	10	6	8	10
# nonzero blocks	14	29	54	14	54	54	14	54	55
# nonzero coefficients	119	195	335	169	670	656	185	841	885
MSEs	0.462	0.451	0.45	0.447	0.439	0.440	0.446	0.439	0.442

Note: For $K = 2$, there are 55 blocks from which 10 are main effects and 45 are two-way interactions. There are a total of 1175 scalar coefficients. For the underlying regression function (49), 14 of the 55 components are true. The MSEs are evaluated on a validation set of $n = 50000$ data points.

Table 2: Sparsity, cross-entropy and misclassification rates for synthetic logistic regression.

$\log_2(\rho^{-1})$	16			19			22		
$\log_2(\lambda^{-1})$	6	8	10	6	8	10	6	8	10
# nonzero blocks	13	46	55	18	55	55	39	55	55
# nonzero coefficients	91	226	258	205	658	655	721	1011	1020
cross-entropy	0.541	0.537	0.536	0.535	0.533	0.534	0.534	0.535	0.537
misclassification (%)	26.92	26.8	26.85	26.62	26.69	26.81	26.58	26.87	27.03

Note: For $K = 2$, there are 55 blocks from which 10 are main effects and 45 are two-way interactions. There are a total of 1175 scalar coefficients. For the underlying regression function (49), 14 of the 55 components are true. The cross-entropy and misclassification rates are evaluated on a validation set of $n = 50000$ data points.

$f(X)$ is defined as (49). Note that (X_8, X_9, X_{10}) are spurious inputs. We apply the logistic DPAM (7), with differentiation order $m = 2$ (i.e., piecewise cross-linear basis functions), interaction order $K = 2$ (main effects and two-way interactions), and 6 marginal knots (5 basis functions for each main effect), similarly as in Section 5.2.1. The performances of various algorithms are reported in Figure 3 under different choices of $\rho \in \{2^{-16}, 2^{-19}, 2^{-22}\}$ and $\lambda \in \{\|\tilde{Y}\|_n/2^6, \|\tilde{Y}\|_n/2^8, \|\tilde{Y}\|_n/2^{10}\}$, where \tilde{Y} is the centered version of Y . For solutions from AS-BDT (after convergence declared), the sparsity levels, the cross-entropy and the misclassification rates under different tuning parameters are summarized in Table 2. The sparsity levels from stochastic primal-dual algorithms are reported in Supplement Table S3.

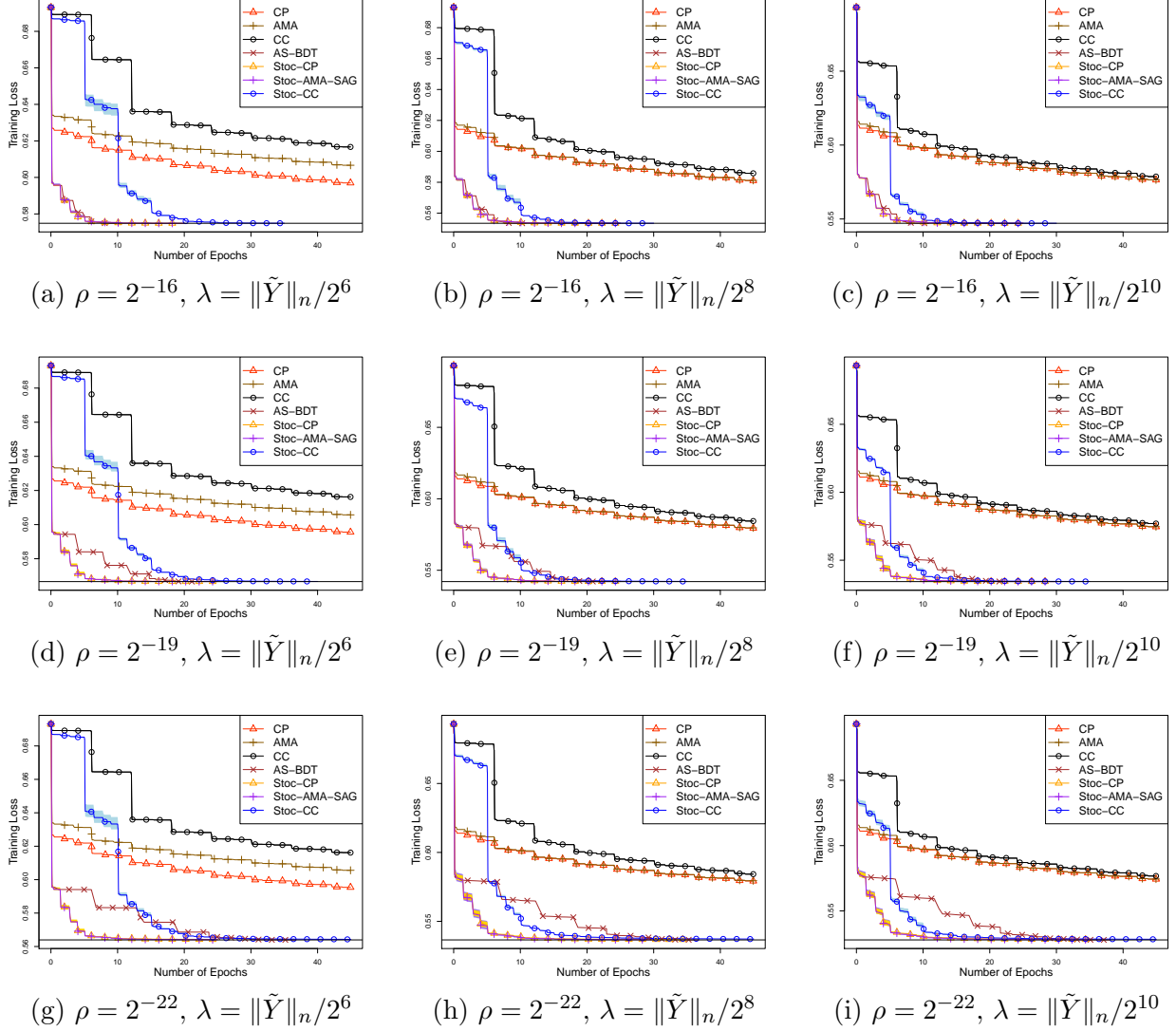


Figure 3: DPAM training in synthetic logistic regression. The minimal training loss achieved from AS-BDT is given by the black solid line. For the stochastic algorithms, we plot the mean as well as the minimum and maximum training losses across 10 repeated runs.

A tolerance of 10^{-4} in the objective value (average log-likelihood) is checked after each backfitting cycle over all blocks to declare convergence.

5.2.3 Logistic regression on real data

We evaluate the performances of various algorithms on a real dataset, run-or-walk, where the aim is to classify whether a person is running or walking based on sensor data collected from an iOS device. The dataset is available from Kaggle <https://www.kaggle.com/datasets/>

`vmalyi/run-or-walk`. The run-or-walk dataset has 88588 data points, 6 explanatory variables and 1 binary response variable. The 6 explanatory variables (acc_x , acc_y , acc_z , $gyro_x$, $gyro_y$ and $gyro_z$) are collected from the accelerometer and gyroscope in 3 dimensions. The binary variable Y indicates whether the person is running (1) or walking (0).

For pre-processing, we standardize the 6 explanatory variables by subtracting their sample means and then dividing by their sample standard deviations. Then we split the data randomly into a training set of size $n = 70870$ (around 80% of the full dataset) and a validation set of size 17718, to mimic a 5-fold cross-validation. We apply the logistic DPAM (7), with differentiation order $m = 2$ (i.e., piecewise cross-linear basis functions), interaction order $K = 2$ (main effects and two-way interactions), and 6 marginal knots (5 basis functions for each main effect), as in Section 5.2.2. The performances of various algorithms are reported in Figure 4 under different choices of $\rho \in \{2^{-18}, 2^{-23}, 2^{-25}\}$ and $\lambda \in \{\|\tilde{Y}\|_n/2^6, \|\tilde{Y}\|_n/2^{13}, \|\tilde{Y}\|_n/2^{15}\}$, where \tilde{Y} is the centered version of Y . For solutions from AS-BDT (after convergence declared), the sparsity levels, the cross-entropy and the misclassification rates under different tuning parameters are summarized in Table 3. An objective tolerance of 10^{-4} is checked in the average log-likelihood after each cycle over all blocks to declare convergence.

Table 3: Sparsity, cross-entropy and misclassification rates for logistic regression on real data.

$\log_2(\rho^{-1})$	18			23			25		
$\log_2(\lambda^{-1})$	6	13	15	6	13	15	6	13	15
# nonzero blocks	17	21	21	19	21	21	19	21	21
# nonzero coefficients	220	240	239	313	332	333	307	336	334
cross-entropy (in 10^{-2})	8.93	6.57	6.56	8.06	5.55	5.54	8.00	5.56	5.56
misclassification (%)	1.95	1.71	1.71	1.86	1.53	1.53	1.89	1.58	1.57

Note: For $K = 2$, there are 21 blocks from which 6 are main effects and 15 are two-way interactions. There are a total of 405 scalar coefficients. The cross-entropy and misclassification rates are evaluated on the validation set.

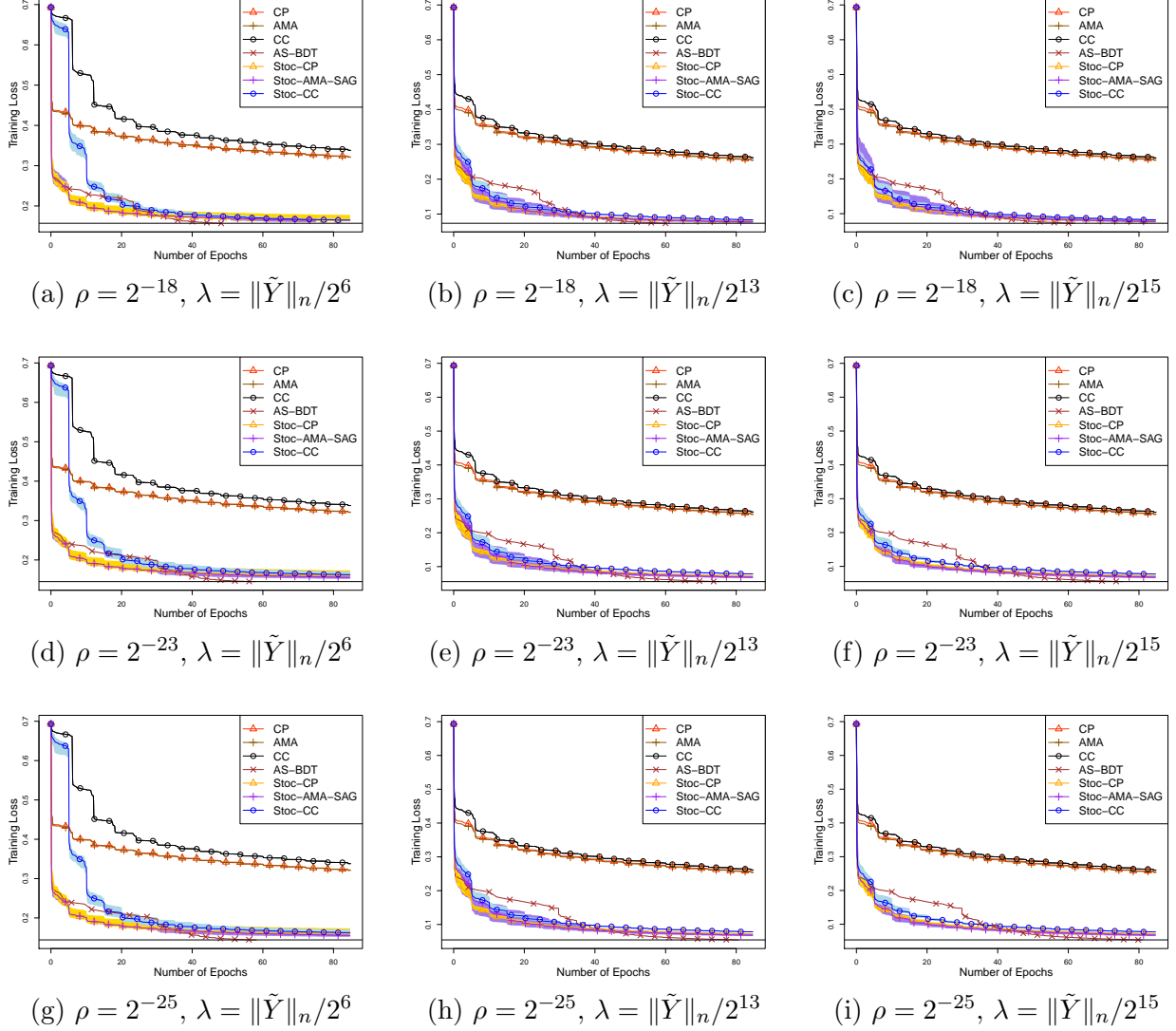


Figure 4: DPAM training in logistic regression on real data. The minimal training loss achieved from AS-BDT is given by the black solid line. For the stochastic algorithms, we plot the mean as well as the minimum and maximum training losses across 10 repeated runs.

5.2.4 Comparisons

From Figures 2–4 as well as Figures S3 and S4 for the phase shift model in the Supplement, we observe the following trends.

- **Batch vs Stochastic:** Compared with their batch counterparts, all three stochastic algorithms (Stoc-CP, and Stoc-AMA-SAG, Stoc-CC) achieve considerable improvements. Due to the non-descent nature, batch primal-dual algorithms require more iterations in each block, so that the overall performances are compromised. However,

stochastic primal-dual algorithms are less affected by this downside, which can also be seen from the advantages over batch versions in single-block optimization (Figure 1).

- **Stochastic primal-dual algorithms:** Stochastic primal-dual algorithms perform better than or similarly as Stoc-CC. Comparison between stochastic primal-dual algorithms and AS-BDT depends on the penalty parameter ρ , which controls the element-wise sparsity of the solution. Their performances are similar for relatively large ρ . As ρ decreases (leading to less sparse solutions), the stochastic primal-dual algorithms achieve a significant advantage over AS-BDT (except in Figure 4 where the acceleration of AS-BDT takes effect as discussed below).
- **Stoc-CC:** The performance of Stoc-CC seems to be sensitive to the penalty parameter λ , which controls the block-wise sparsity. The performance improves as λ decreases. A similar pattern can also be observed on batch CC. A heuristic explanation is that when λ is small, the solutions β in the nonzero blocks may deviate more from 0 such that the majorization in CC captures the local curvature more accurately (as illustrated in Figure S2). See Supplement Section II for further discussion.
- **Acceleration of AS-BDT:** In Figure 4, the stochastic algorithms are more efficient at the beginning, but are slightly outperformed by AS-BDT as training continues. Such acceleration occurs because AS-BDT exploits the active-set information from the previous cycle to achieve computational savings, which can be substantial as many cycles of backfitting are run in logistic regression where quadratic approximations are involved. In fact, in Figure 4, while the three stochastic algorithms go through at most 16 cycles of backfitting in a 80-epoch run, the number of backfitting cycles completed by AS-BDT are as large as 30. This observation suggests a hybrid strategy combining AS-BDT and stochastic algorithms, as discussed in Section 4.2.
- **Variance:** The three stochastic algorithms have almost invisible variances in Figures 2 and 3. In Figure 4, the stochastic Chambolle–Pock algorithm tends to have smaller variances than the other two for small λ (leading to block-wise denser solutions).

6 Conclusion

We develop two primal-dual algorithms, including both batch and stochastic versions, for doubly-penalized ANOVA modeling with both HTV and empirical-norm penalties, where existing primal-dual algorithms are not suitable. Our numerical experiments demonstrate considerable gains from the stochastic primal-dual algorithms compared with their batch versions and the previous algorithm AS-BDT in large-scale, especially non-sparse, scenarios. Nevertheless, theoretical convergence remains to be studied. Moreover, a hybrid approach can be explored by combining stochastic primal-dual and AS-BDT algorithms.

References

- Bottou, L., Curtis, F. E., & Nocedal, J. (2018). Optimization methods for large-scale machine learning. *SIAM Review*, *60*, 223–311.
- Boyd, S., Parikh, N., Chu, E., Peleato, B., & Eckstein, J. (2011). Distributed optimization and statistical learning via the alternating direction method of multipliers. *Foundations and Trends in Machine Learning*, *3*, 1–122.
- Chambolle, A., & Pock, T. (2011). A first-order primal-dual algorithm for convex problems with applications to imaging. *Journal of Mathematical Imaging and Vision*, *40*, 120–145.
- Chen, P., Huang, J., & Zhang, X. (2013). A primal–dual fixed point algorithm for convex separable minimization with applications to image restoration. *Inverse Problems*, *29*, 025011.
- Condat, L. (2013). A primal–dual splitting method for convex optimization involving Lipschitzian, proximable and linear composite terms. *Journal of Optimization Theory and Applications*, *158*, 460–479.
- Defazio, A., Bach, F., & Lacoste-Julien, S. (2014). SAGA: A fast incremental gradient method with support for non-strongly convex composite objectives. *Advances in Neural Information Processing Systems*, *27*.
- Drori, Y., Sabach, S., & Teboulle, M. (2015). A simple algorithm for a class of nonsmooth convex–concave saddle-point problems. *Operations Research Letters*, *43*, 209–214.
- Esser, E., Zhang, X., & Chan, T. F. (2010). A general framework for a class of first order

- primal-dual algorithms for convex optimization in imaging science. *SIAM Journal on Imaging Sciences*, *3*, 1015–1046.
- Friedman, J. (1991). Multivariate adaptive regression splines (with discussion). *Annals of Statistics*, *19*, 79–141.
- Gu, C. (2013). *Smoothing Spline ANOVA Models* (Second ed.). Springer.
- Hastie, T., & Tibshirani, R. (1990). *Generalized Additive Models*. Taylor & Francis.
- Hunter, D. R., & Lange, K. (2004). A tutorial on MM algorithms. *American Statistician*, *58*, 30–37.
- Koltchinskii, V., & Yuan, M. (2010). Sparsity in multiple kernel learning. *Annals of Statistics*, *38*, 3660–3695.
- Li, Z., & Yan, M. (2021). New convergence analysis of a primal-dual algorithm with large stepsizes. *Advances in Computational Mathematics*, *47*, 1–20.
- Lin, Y., & Zhang, H. H. (2006). Component selection and smoothing in multivariate non-parametric regression. *Annals of Statistics*, *34*, 2272–2297.
- Mammen, E., & Van De Geer, S. (1997). Locally adaptive regression splines. *Annals of Statistics*, *25*, 387–413.
- Meier, L., Van de Geer, S., & Bühlmann, P. (2009). High-dimensional additive modeling. *Annals of Statistics*, *37*, 3779–3821.
- Osborne, M. R., Presnell, B., & Turlach, B. A. (2000). A new approach to variable selection in least squares problems. *IMA Journal of Numerical Analysis*, *20*, 389–403.
- Parikh, N., & Boyd, S. (2014). Proximal algorithms. *Foundations and Trends in Optimization*, *1*, 127–239.
- Petersen, A., Witten, D., & Simon, N. (2016). Fused lasso additive model. *Journal of Computational and Graphical Statistics*, *25*, 1005–1025.
- Radchenko, P., & James, G. M. (2010). Variable selection using adaptive nonlinear interaction structures in high dimensions. *Journal of the American Statistical Association*, *105*, 1541–1553.
- Raskutti, G., Wainwright, M. J., & Yu, B. (2012). Minimax-optimal rates for sparse additive models over kernel classes via convex programming. *Journal of Machine Learning*

Research, 13.

- Ravikumar, P., Lafferty, J., Liu, H., & Wasserman, L. (2009). Sparse additive models. *Journal of the Royal Statistical Society, Series B*, 71, 1009–1030.
- Roux, N., Schmidt, M., & Bach, F. (2012). A stochastic gradient method with an exponential convergence rate for finite training sets. *Advances in Neural Information Processing Systems*, 25.
- Ryu, E. K., & Yin, W. (2022). *Large-Scale Convex Optimization via Monotone Operators*. Cambridge University Press.
- Stone, C. J. (1986). The dimensionality reduction principle for generalized additive models. *Annals of Statistics*, 590–606.
- Tan, Z., & Zhang, C.-H. (2019). Doubly penalized estimation in additive regression with high-dimensional data. *Annals of Statistics*, 47, 2567–2600.
- Tseng, P. (1988). Coordinate ascent for maximizing nondifferentiable concave functions. *Technical Report LIDS-P-1840, MIT*.
- Tseng, P. (1991). Applications of a splitting algorithm to decomposition in convex programming and variational inequalities. *SIAM Journal on Control and Optimization*, 29, 119–138.
- Vũ, B. C. (2013). A splitting algorithm for dual monotone inclusions involving cocoercive operators. *Advances in Computational Mathematics*, 38, 667–681.
- Wahba, G., Wang, Y., Gu, C., Klein, R., & Klein, B. (1995). Smoothing spline ANOVA for exponential families, with application to the Wisconsin Epidemiological Study of Diabetic Retinopathy. *Annals of Statistics*, 23, 1865–1895.
- Yang, T., & Tan, Z. (2018). Backfitting algorithms for total-variation and empirical-norm penalized additive modelling with high-dimensional data. *Stat*, 7, e198.
- Yang, T., & Tan, Z. (2021). Hierarchical total variations and doubly penalized ANOVA modeling for multivariate nonparametric regression. *Journal of Computational and Graphical Statistics*, 30, 848–862.
- Zhang, Y., & Xiao, L. (2017). Stochastic primal-dual coordinate method for regularized empirical risk minimization. *Journal of Machine Learning Research*, 18, 1–42.

Supplementary Material for
 “Block-wise Primal-dual Algorithms for Large-scale Doubly
 Penalized ANOVA Modeling”

Penghui Fu and Zhiqiang Tan

I Three-operator splitting method

Condat–Vũ (Condat, 2013; Vũ, 2013) is a three-operator splitting method which can be viewed as a generalization of the Chambolle–Pock and proximal gradient method. Consider an optimization problem in the form

$$\min_{\beta} \tilde{h}(\beta) + \tilde{g}(\beta) + \tilde{f}(X\beta), \quad (\text{S1})$$

where \tilde{h} , \tilde{g} , and \tilde{f} are CCP functions, and \tilde{h} is L -smooth. The primal-dual Lagrangian associated with (S1) is

$$L(\beta; u) = \tilde{h}(\beta) + \tilde{g}(\beta) + \langle u, X\beta \rangle - \tilde{f}^*(u). \quad (\text{S2})$$

Then the dual problem of (S1) is $\max_u -(\tilde{h} + \tilde{g})^*(-X^\top u) - \tilde{f}^*(u)$. For solving (S1), Condat–Vũ iterations are defined as follows: for $k \geq 0$,

$$\begin{aligned} \beta^{k+1} &= \mathbf{prox}_{\tau\tilde{g}/n} \left(\beta^k - \frac{\tau}{n}(X^\top u^k + \nabla\tilde{h}(\beta^k)) \right), \\ u^{k+1} &= \mathbf{prox}_{\alpha\tilde{f}^*} \left(u^k + \alpha X(2\beta^{k+1} - \beta^k) \right). \end{aligned} \quad (\text{S3})$$

If $\tilde{h} = 0$, then (S3) becomes the Chambolle–Pock method (16). If $\tilde{f} = 0$, then (S3) becomes the proximal gradient method (18), because $\tilde{f}^*(u) = \delta_{\{0\}}(u)$ and consequently $u^{k+1} = 0$. Therefore, Condat–Vũ generalizes the CP and proximal gradient method. Assuming that total duality holds, $\alpha > 0$, $\tau > 0$, and $(\alpha + 1/2)\tau L < n$, then the iterates (β^{k+1}, u^{k+1}) in (S3) converge to a saddle point of (S2) (Ryu & Yin, 2022).

To apply Condat–Vũ, we reformulate the single-block problem (23) as

$$\min_{\beta} \underbrace{\frac{1}{2}\|r - X\beta\|_2^2}_{\tilde{h}(\beta)} + \underbrace{n\|\Gamma\beta\|_1}_{\tilde{g}(\beta)} + \underbrace{\lambda\sqrt{n}\|X\beta\|_2}_{\tilde{f}(X\beta)}, \quad (\text{S4})$$

where $\tilde{h}(\beta) = \|r - X\beta\|_2^2/2$ is $\|X\|_2^2$ -smooth, $\tilde{g}(\beta) = n\|\Gamma\beta\|_1$, and $\tilde{f}(z) = \lambda\sqrt{n}\|z\|_2$ for $z \in \mathbb{R}^n$. The conjugate $\tilde{f}^*(u)$ can be calculated in a closed form as $\tilde{f}^*(u) = \delta(\|u\|_2 \leq \lambda\sqrt{n})$.

Applying Condat–Vũ (S3) to problem (S4), we obtain

$$\beta^{k+1} = \mathbf{prox}_{\tau\tilde{g}/n} \left(\beta^k - \frac{\tau}{n} (X^\top u^k + \nabla\tilde{h}(\beta^k)) \right) \quad (\text{S5a})$$

$$= \mathcal{S} \left(\beta^k - \frac{\tau}{n} X^\top (u^k + X\beta^k - r), \tau \text{diag}(\Gamma) \right), \quad (\text{S5b})$$

$$u^{k+1} = \mathbf{prox}_{\alpha\tilde{f}^*} (u^k + \alpha X(2\beta^{k+1} - \beta^k)) \quad (\text{S5c})$$

$$= \prod_{\{z: \|z\|_2 \leq \lambda\sqrt{n}\}} (u^k + \alpha X(2\beta^{k+1} - \beta^k)), \quad (\text{S5d})$$

where $\prod_{\{z: \|z\|_2 \leq \lambda\sqrt{n}\}}$ is the orthogonal projection onto the set $\{z \in \mathbb{R}^n: \|z\|_2 \leq \lambda\sqrt{n}\}$. By the preceding discussion, the iterates (β^{k+1}, u^{k+1}) in (S5) converge to a saddle point of (S2) provided that $\alpha > 0$, $\tau > 0$, and $(\alpha + 1/2)\tau\|X\|_2^2 < n$.

While the batch algorithm (S5) is tractable, a proper randomization of the algorithm seems to be difficult. The randomization techniques used in Sections 3.2.1 and 3.2.2 are not applicable for deriving a randomized version of the dual update (S5d), which will be denoted as u_{B}^{k+1} . On one hand, \tilde{f}^* above is not separable, so that evaluating one coordinate of u_{B}^{k+1} has a cost of $O(nd)$, the same as that of evaluating the full update. The randomized coordinate update which is unbiased for u_{B}^{k+1} as in stochastic linearized AMA is infeasible. On the other hand, \tilde{f}^* is not differentiable either. Hence a randomized coordinate minimization update as used in stochastic CP may not be valid (Tseng, 1988).

II Concave conjugate method

In Sections 3.1 and 3.2, the single-block optimization problem (23) is solved through a saddle-point problem by using primal-dual methods. In fact, we replace $f(X\beta) = (1/2)\|r - X\beta\|_2^2 + \lambda\sqrt{n}\|X\beta\|_2$ by its Fenchel conjugate

$$f(X\beta) = \max_u \langle u, X\beta \rangle - f^*(u),$$

and keep $g(\beta) = n\|\Gamma\beta\|_1$ unchanged. Then the original problem (23) is transformed to the min-max (i.e., saddle-point) problem of the Lagrangian

$$\min_{\beta} \max_u L(\beta, u) = g(\beta) + \langle u, X\beta \rangle - f^*(u).$$

In this section, we present a different approach by considering the conjugate of the square root, which is a concave function. This transforms (23) to a min-inf problem, in contrast with the min-max problem using primal-dual methods.

II.1 Concave conjugate and MM

By Fenchel duality on the square root function, we have

$$\sqrt{x} = \inf_{u < 0} (\psi^*(u) - ux), \quad x \geq 0, \quad (\text{S6})$$

where $\psi^*(u) = -1/(4u)$ if $u < 0$ and ∞ otherwise. The optimal $u(x)$ achieving the infimum is $-1/(2\sqrt{x})$ if $x > 0$ and $-\infty$ if $x = 0$. By (S6), problem (21) is equivalent to

$$\min_{\beta} \inf_{u < 0} \frac{1}{2n} \|r - X\beta\|_2^2 + \|\Gamma\beta\|_1 + \lambda(\psi^*(u) - u\|X\beta\|_n^2). \quad (\text{S7})$$

Naturally, we consider alternately minimizing or decreasing the objective in (S7) with respect to u and β . For fixed $\beta \neq 0$, the optimal u is given by $\hat{u}(\beta) = -1/(2\|X\beta\|_n)$. For fixed u , minimization over β is equivalent to, after rescaling by $1/(1 - 2\lambda u) > 0$,

$$\min_{\beta} \frac{1}{2n} \|X\beta - \frac{1}{1 - 2\lambda u} r\|_2^2 + \frac{1}{1 - 2\lambda u} \|\Gamma\beta\|_1. \quad (\text{S8})$$

Note that (S8) is a Lasso problem similar to (22), but with r and Γ rescaled. By the min-inf structure of (S7), any update of β decreasing the objective in (S8) with $u = \hat{u}(\beta^k)$ given the current β^k can be shown to also reduce the objective in the original problem (21). For example, consider a proximal gradient update as in (18)

$$\beta^{k+1} = \mathcal{S} \left(\beta^k - \frac{\tau}{n} X^T (X\beta^k - \frac{1}{1 - 2\lambda u} r), \frac{\tau}{1 - 2\lambda u} \cdot \text{diag}(\Gamma) \right). \quad (\text{S9})$$

For $0 < \tau \leq n/\|X\|_2^2$, this update is guaranteed to decrease the objective in (S8) and hence also the objective in problem (21) (Parikh & Boyd, 2014).

The alternate updating procedure above will be called concave conjugate (CC), to reflect our original motivation. Interestingly, the procedure can also be interpreted as an MM algorithm (Hunter & Lange, 2004). The basic idea of MM is to replace an objective function $h(\beta)$ by a suitable surrogate $\tilde{h}(\beta, \beta^k)$ at the current β^k . The surrogate is called a majorization if the surrogate contacts the original objective at β^k , $\tilde{h}(\beta^k, \beta^k) = h(\beta^k)$, and is an upper bound, $\tilde{h}(\beta, \beta^k) \geq h(\beta)$ for all β . If the surrogate is a majorization, then any β^{k+1} that decreases $\tilde{h}(\beta, \beta^k)$ will also decrease h , i.e., $h(\beta^{k+1}) \leq h(\beta^k)$.

The objective in (S7) with $u = \hat{u}(\beta^k)$ can be shown to provide a majorization function at β^k for the objective in the original problem (21). In fact, a majorization function for $\|X\beta\|_n$ is constructed as follows:

$$\|X\beta\|_n \leq \left\{ \psi^*(u) - u\|X\beta\|_n^2 \right\} \Big|_{u=\hat{u}(\beta^k)}$$

$$= \frac{1}{2\sqrt{\|X\beta^k\|_n^2}}(\|X\beta\|_n^2 - \|X\beta^k\|_n^2) + \sqrt{\|X\beta^k\|_n^2}.$$

For $x = \|X\beta\|_n^2$, the preceding display can be stated directly as a linear majorization of the square root function \sqrt{x} at $x^k = \|X\beta^k\|_n^2$:

$$\sqrt{x} \leq \frac{1}{2\sqrt{x^k}}(x - x^k) + \sqrt{x^k}, \quad (\text{S10})$$

See Figure S1 for an illustration. Equivalently, (S10) can be expressed as a quadratic majorization of the absolute function $|t|$ at some t^k :

$$|t| \leq \frac{1}{2|t^k|}(t^2 - (t^k)^2) + |t^k|. \quad (\text{S11})$$

See Figure S2 for an illustration. Quadratic majorizations related to (S11) were used in Hunter & Li (2005) to derive MM algorithms for handling non-concave penalties.

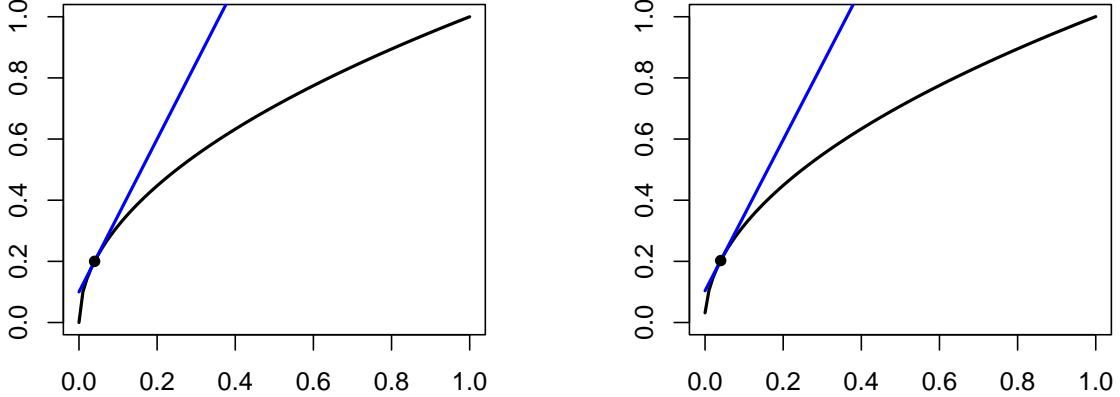


Figure S1: Linear majorizations of \sqrt{x} and $\sqrt{x + 0.001}$ at $x = 0.04$.

A major limitation of CC or MM discussed above is that the procedure would break down when $\beta^k = 0$. From the CC perspective, if $\beta^k = 0$, the associated $\hat{u}(\beta^k)$ becomes $-\infty$, so that β^{k+1} would stay at 0, even when the solution for β is nonzero. From the MM perspective, the majorization in (S10) or (S11) becomes improper if $x^k = 0$ or $t^k = 0$.

To address this issue, a possible approach is to add a small perturbation to the empirical norm, that is, modifying the objective in (21) to

$$\frac{1}{2n}\|r - X\beta\|_2^2 + \|\Gamma\beta\|_1 + \lambda\sqrt{\|X\beta\|_n^2 + \delta}, \quad (\text{S12})$$

for some small $\delta > 0$. For the alternate updating procedure, the u step leads to $\hat{u}_\delta(\beta) = -1/(2\sqrt{\|X\beta\|_n^2 + \delta}) > -\infty$. The proximal gradient update for β remains the same as (S9),

but with u set to $\hat{u}_\delta(\beta)$. As illustrated in Figures S2 and S1, the corresponding majorization can be stated as

$$\sqrt{x + \delta} \leq \frac{1}{2\sqrt{x^k + \delta}}(x - x^k) + \sqrt{x^k + \delta},$$

for $x = \|X\beta\|_n^2$, or equivalently

$$\sqrt{t^2 + \delta} \leq \frac{1}{2\sqrt{(t^k)^2 + \delta}}(t^2 - (t^k)^2) + \sqrt{(t^k)^2 + \delta}.$$

for $t = \pm\|X\beta\|_n$. The resulting CC algorithm is presented in Algorithm S1. For easy comparison with other algorithms, the updates are also expressed as (S13) and (S14). The step size τ^k in (S13) corresponds to the choice $\tau = n/\|X\|_2^2$ in (S9) to guarantee descent of the objective, and the β -update in (S14) is re-expressed from (S9) with $u = \hat{u}_\delta(\beta^k)$ absorbed.

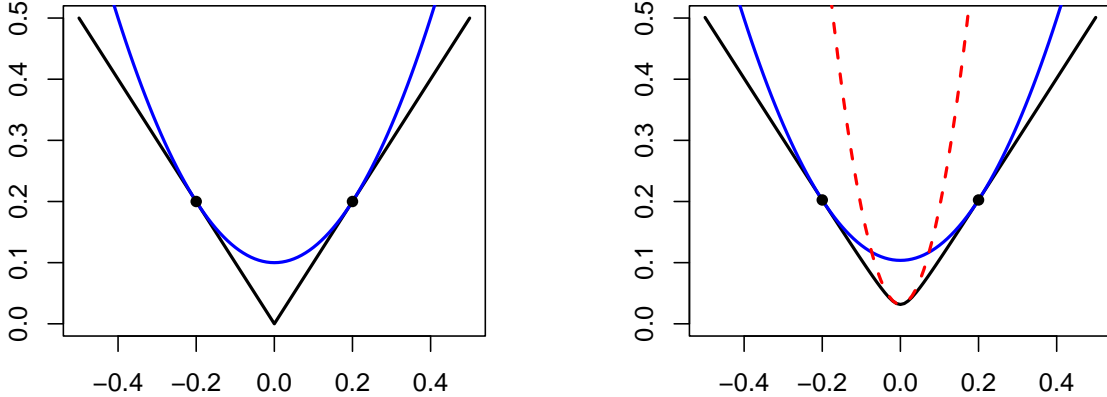


Figure S2: Quadratic majorizations of $|t|$ and $\sqrt{t^2 + 0.001}$ at $t = 0.2$. The red dotted curve is the quadratic majorization of $\sqrt{t^2 + 0.001}$ at $t = 0$.

A stochastic version of batch CC is presented in Algorithm S2, with outer and inner loops. Given the current β^k in the outer loop, u is updated as $\hat{u}_\delta(\beta^k)$ and then SAGA is applied in an inner loop to the proximal gradient update (S9) for β , with $u = \hat{u}_\delta(\beta^k)$ fixed. Each inner iteration costs $O(d)$. Therefore, one outer iteration with an inner loop of n iterations costs $O(nd)$, the same as one batch step in Algorithm S1.

Algorithm S1 Single-block Batch CC

Input Initial β^0 , number of batch steps B , perturbation δ .

for $k = 0, \dots, B - 1$ **do**

Set $\tau = n/\|X\|_2^2$. Perform the following updates:

$$\begin{aligned} u^{k+1} &= \hat{u}_\delta(\beta^k) = -1/(2\sqrt{\|X\beta^k\|_n^2 + \delta}), \\ \beta^{k+1} &= \mathcal{S} \left(\beta^k - \frac{\tau}{n} X^\top (X\beta^k - \frac{1}{1 - 2\lambda u^{k+1}} r), \frac{\tau}{1 - 2\lambda u^{k+1}} \cdot \text{diag}(\Gamma) \right). \end{aligned}$$

Equivalently, the updates can be expressed as

$$\tau^k = \frac{n/\|X\|_2^2}{(1 + \lambda/\sqrt{\|X\beta^k\|_n^2 + \delta})}, \quad (\text{S13})$$

$$\beta^{k+1} = \mathcal{S} \left(\beta^k - \frac{\tau^k}{n} X^\top \left(X\beta^k - r + \frac{\lambda X\beta^k}{\sqrt{\|X\beta^k\|_n^2 + \delta}} \right), \tau^k \cdot \text{diag}(\Gamma) \right). \quad (\text{S14})$$

II.2 Comparison with proximal gradient method

After the empirical norm is modified, the perturbed objective (S12) becomes amenable to a broader range of methods in convex optimization, for example, the proximal gradient method, the proximal Newton method, and so on. We compare CC with the proximal gradient method applied directly to (S12) with a constant step size, and show that the majorization allows the proximal gradient step in CC to adapt to the local curvature.

The perturbed objective (S12) can be split into two terms: the differentiable term $h_1(\beta) = \|r - X\beta\|_n^2/2 + \lambda\sqrt{\|X\beta\|_n^2 + \delta}$ and the non-differentiable term $h_2(\beta) = \|\Gamma\beta\|_1$. With this split, the proximal gradient method can be applied directly to minimize (S12). The β -update can be shown to be of the same form as (S14) in Algorithm S1, but with the step size τ^k in (S13) replaced by a constant τ . To guarantee convergence, the choice of the step size τ depends on the global curvature/smoothness of the differentiable term $h_1(\beta)$.

Proposition S1. *Let $h_0(z) = \lambda\sqrt{\|z\|_2^2 + \delta}$. Then h_0 is $\lambda/\sqrt{\delta}$ -smooth:*

$$\|\nabla h_0(x) - \nabla h_0(y)\|_2 \leq (\lambda/\sqrt{\delta})\|x - y\|_2, \quad \forall x, y.$$

As a result, $h_1(\beta) = \|r - X\beta\|_n^2/2 + \lambda\sqrt{\|X\beta\|_n^2 + \delta}$ is $(1 + \lambda/\sqrt{\delta})\|X\|_2^2/n$ -smooth.

Algorithm S2 Single-block Stochastic CC-SAGA

Input Initial β^0 , number of batch steps B , step size τ , perturbation δ .

for $k = 0, \dots, B - 1$ **do**

Update

$$u^{k+1} = \hat{u}_\delta(\beta^k) = -\frac{1}{2\sqrt{\|X\beta^k\|_n^2 + \delta}}.$$

Set $v^0 = X\beta^k - r/(1 - 2\lambda u^k)$, $w^0 = X^\top v^0/n$, and $\tilde{\beta}^0 = \beta^k$.

for $s = 0, \dots, n - 1$ **do**

Pick i uniformly from $\{1, \dots, n\}$, and perform the following updates:

$$\begin{aligned} v_i^{s+1} &= X_{i,\cdot}^\top \beta^s - r_i/(1 - 2\lambda u^k) \quad \text{or} \quad v_j^{s+1} = v_j^s \text{ for } j \neq i, \\ \tilde{\beta}^{s+1} &= \mathcal{S} \left(\tilde{\beta}^s - \tau (w^s + X_{i,\cdot} (v_i^{s+1} - v_i^s)), \frac{\tau}{1 - 2\lambda u^k} \cdot \text{diag}(\Gamma) \right), \\ w^{s+1} &= w^s + X_{i,\cdot} (v_i^{s+1} - v_i^s)/n. \end{aligned}$$

Update $\beta^{k+1} = \tilde{\beta}^n$.

From Proposition S1, the step size of the proximal gradient method should be no greater than $n/\{(1 + \lambda/\sqrt{\delta})\|X\|_2^2\}$, to ensure descent of the objective (Parikh & Boyd, 2014). By comparison, the varying step size τ^k in (S13) is no smaller than $n/\{(1 + \lambda/\sqrt{\delta})\|X\|_2^2\}$ and can be considerably larger if $\|X\beta^k\|_n^2 \gg \delta$.

This phenomenon can be explained geometrically. As seen from Figure S2, the quadratic majorization captures the local curvature of $\sqrt{t^2 + \delta}$, depending on the current point t^k : it becomes flatter as $|t^k|$ is larger, and is sharpest at the origin. Hence the implied step size τ^k for the proximal gradient in Algorithm S1 can be adaptive to the local curvature. In contrast, the direct proximal gradient uses a constant global curvature, which corresponds to the largest curvature (at 0). This leads to a smaller (conservative) step size and hence a slower convergence if the solution for β is far away from 0.

III Technical details

III.1 Relation between linearized ADMM and CP

We derive the Chambolle–Pock (CP) algorithm (16) from linearized ADMM (15). By (15a) and Moreau’s identity (8), we have

$$z^{k+1} = Ax^k + u^k/\alpha - \mathbf{prox}_{\alpha f^*}(\alpha Ax^k + u^k)/\alpha. \quad (\text{S15})$$

Let $v^{k+1} = \mathbf{prox}_{\alpha f^*}(\alpha Ax^k + u^k)$, which is (17a). Then (S15) becomes

$$z^{k+1} = Ax^k + u^k/\alpha - v^{k+1}/\alpha. \quad (\text{S16})$$

Substituting (S16) into (15b), we obtain (16b). Combining (S16) with $u^{k+1} = u^k + \alpha(Ax^{k+1} - z^{k+1})$ in (15) we have

$$u^{k+1} = \alpha A(x^{k+1} - x^k) + v^{k+1}. \quad (\text{S17})$$

If $u^0 = \alpha A(x^0 - x^{-1}) + v^0$, then (S17) holds for $k \geq -1$. Hence we obtain (17b). Substituting (S17) into the definition of v^{k+1} , we obtain (16a). Collecting (16a) and (16b) yields the CP algorithm.

For matching between linear ADMM and CP, based on the reasoning above, (v^{k+1}, x^{k+1}) in CP (16) can be recovered from linearized ADMM (15) as $(\mathbf{prox}_{\alpha f^*}(\alpha Ax^k + u^k), x^{k+1})$ or $(u^k + \alpha(Ax^k - z^{k+1}), x^{k+1})$ for all $k \geq 0$. Reversely, $(z^{k+1}, x^{k+1}, u^{k+1})$ in linearized ADMM (15) can be recovered from CP (16) as $(A(2x^k - x^{k-1}) + (v^k - v^{k+1})/\alpha, x^{k+1}, \alpha A(x^{k+1} - x^k) + v^{k+1})$, for all $k \geq 0$.

For completeness, we briefly discuss the relation between re-ordered linearized ADMM and a dual version of CP. After exchanging the order of (15a) and (15b), through a similar argument as above, the re-ordered linearized ADMM can be simplified as

$$\begin{aligned} x^{k+1} &= \mathbf{prox}_{\tau g}(x^k - \tau A^T(2u^k - u^{k-1})), \\ u^{k+1} &= \mathbf{prox}_{\alpha f^*}(u^k + \alpha Ax^{k+1}), \end{aligned} \quad (\text{S18})$$

with z^{k+1} absorbed. It can be shown that (S18) is equivalent to CP (16) applied to the dual problem (12). Compared with the original CP (16), both the update order of primal and dual variables and the extrapolation are flipped in (S18).

III.2 Proof of Proposition 1

Applying PAPC/PDFP²O to the dual problem (12), we obtain

$$\begin{aligned} x^{k+1} &= \mathbf{prox}_{\tau g}(x^k - \tau A^T(u^k - \alpha \nabla f^*(u^k) + \alpha Ax^k)), \\ u^{k+1} &= u^k - \alpha \nabla f^*(u^k) + \alpha Ax^{k+1}. \end{aligned}$$

Letting $z^{k+1} = \nabla f^*(u^k)$, we immediately recover (20).

For the convergence, by Theorem 2 in Li & Yan (2021), if $0 < \alpha < 2\mu$ and $0 < \alpha\tau\|A\|_2^2 \leq 4/3$, then u^{k+1} converges to u^* which is optimal for (12), and x^{k+1} converges to $x^* \in \partial g^*(-A^T u^*)$ such that $\nabla f^*(u^*) - Ax^* = 0$. Let $z^* = \nabla f^*(u^*)$. Then (z^*, x^*, u^*) is a saddle point for (11). By the continuity of ∇f^* , z^{k+1} converges to $\nabla f^*(u^*) = z^*$. Hence $(z^{k+1}, x^{k+1}, u^{k+1})$ converges to (z^*, x^*, u^*) , as desired.

III.3 Proof of Proposition 4

The coordinate descent problem is to solve

$$\operatorname{argmin}_{v_i} \frac{1}{2}(v_i - b_i)^2 + \alpha f^*(v_i, v_{-i}^k),$$

which is the proximal mapping of f^* with respect to a single coordinate v_i . Since f^* is closed, convex and proper, the proximal mapping uniquely exists, and we denote it as v_i^* . Because f^* is smooth, it suffices to solve the first-order condition

$$v_i - b_i + \alpha \left(1 - \frac{\lambda\sqrt{n}}{\sqrt{(v_i + r_i)^2 + \|v^k + r\|_{-i}^2}} \right)_+ (v_i + r_i) = 0. \quad (\text{S19})$$

If $(v_i + r_i)^2 + \|v^k + r\|_{-i}^2 \leq n\lambda^2$, (S19) reduces to $v_i - b_i = 0$, so that $v_i^* = b_i$. Next, assume that $(b_i + r_i)^2 + \|v^k + r\|_{-i}^2 > n\lambda^2$. Then the term inside $(\cdot)_+$ in (S19) must be positive. Let $\tilde{v}_i = v_i + r_i$. Then (S19) becomes

$$b_i + r_i = \left(1 + \alpha - \frac{\alpha\lambda\sqrt{n}}{\tilde{v}_i^2 + \|v^k + r\|_{-i}^2} \right) \tilde{v}_i.$$

If $b_i + r_i = 0$, then $\tilde{v}_i = 0$ by the fact that $\|v^k + r\|_{-i}^2 > n\lambda^2$. If $b_i + r_i \neq 0$, then $\tilde{v}_i \neq 0$ and \tilde{v}_i must take the form of $c(b_i + r_i)$, where $c \neq 0$ is the root of equation

$$\left(1 + \alpha - \frac{\alpha\lambda\sqrt{n}}{\sqrt{c^2(b_i + r_i)^2 + \|v^k + r\|_{-i}^2}} \right) c = 1. \quad (\text{S20})$$

The left-hand side (LHS) of (S20) is strictly increasing on $[0, \infty)$. When $c = 0$ the LHS of (S20) is 0. When $c = 1$, the LHS of (S20) is greater than 1 by the assumption $(b_i + r_i)^2 + \|v^k + r\|_{-i}^2 > n\lambda^2$. Hence there is a unique c^* in $(0, 1)$ which solves (S20). In the case of $\|v^k + r\|_{-i}^2 = 0$ and $(b_i + r_i)^2 > n\lambda^2$, c^* has a close-form expression

$$c^* = \left(1 + \frac{\alpha\lambda\sqrt{n}}{|b_i + r_i|}\right) / (1 + \alpha).$$

III.4 Proof of Proposition S1

By the chain rule, it suffices to show that $h_0(z) = \lambda\sqrt{\|z\|_2^2 + \delta}$ is $(\lambda/\sqrt{\delta})$ -smooth. Without loss of generality, let $\lambda = 1$. Then

$$\nabla h_0(z) = z / \sqrt{\|z\|_2^2 + \delta},$$

and

$$\nabla^2 h_0(z) = c \cdot I - c^3 \cdot zz',$$

where $c = 1/\sqrt{\|z\|_2^2 + \delta} \leq 1/\sqrt{\delta}$. When $z = 0$, $\nabla^2 h_0(0)$ is a rescaled identity matrix $(1/\sqrt{\delta}) \cdot I$. Next assume that $z \neq 0$. Then for any y we have $\nabla^2 h_0(z)y = c \cdot y - c^3 \cdot zz'y$. Let $y = \hat{y} + y^\perp$ where $\hat{y} = zz'y/(z'z)$ is the projection of y on z . Then $zz'y = (z'z) \cdot \hat{y} = \|z\|_2^2 \cdot \hat{y}$, and

$$\begin{aligned} \nabla^2 h_0(z)y &= c \cdot y - c^3 \cdot zz'y = c \cdot y - (c^3 \|z\|_2^2) \cdot \hat{y} \\ &= (c - c^3 \|z\|_2^2) \cdot \hat{y} + c \cdot y^\perp = (\delta c^3) \cdot \hat{y} + c \cdot y^\perp. \end{aligned}$$

Therefore, for any y ,

$$\begin{aligned} \|\nabla^2 h_0(z)y\|_2^2 &= \|(\delta c^3) \cdot \hat{y} + c \cdot y^\perp\|_2^2 = (\delta^2 c^6) \|\hat{y}\|_2^2 + c^2 \|y^\perp\|_2^2 \\ &\leq (\delta^2/\delta^3) \|\hat{y}\|_2^2 + (1/\delta) \|y^\perp\|_2^2 = (1/\delta) \|y\|_2^2. \end{aligned}$$

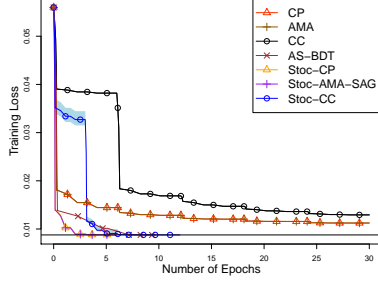
This shows that $\|\nabla^2 h_0(z)\|_2 \leq 1/\sqrt{\delta}$ for all z , which is equivalent to ∇h_0 being $(1/\sqrt{\delta})$ -Lipschitz.

IV Experiments with phase shift model

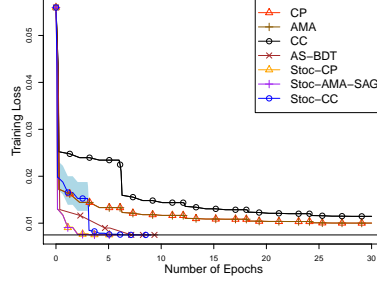
Consider the following example in Friedman (1991), which models the dependence of the phase shift ϕ on the components in a circuit:

$$\phi = \arctan\left(\frac{\omega L - 1/(\omega C)}{R}\right). \quad (\text{S21})$$

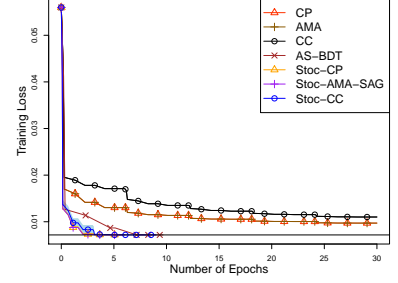
The input variables are independently uniform in the range $0 \leq R \leq 100$, $40\pi \leq \omega \leq 560\pi$, $0 \leq L \leq 1$ and $1 \leq C \leq 11$. We add a normal noise with the standard deviation determined to give a signal-to-noise level 3:1. We first transform the input region to $[0, 1]^4$ and then apply the linear DPAM (6). We take $n = 50000$ and use $m = 2$ (i.e., piecewise cross-linear basis functions) and 11 knots for each raw input. Since all orders of interactions are present in the relationship (S21), we consider both $K = 2$ (up to two-way interactions) and $K = 3$ (up to three-way interactions). The performances of various algorithms are reported in Figures S3 and S4 under different choices of $\rho \in \{2^{-17}, 2^{-21}, 2^{-25}\}$, $\lambda \in \{\|\tilde{\phi}\|_n/2^7, \|\tilde{\phi}\|_n/2^9, \|\tilde{\phi}\|_n/2^{11}\}$ for $K = 2$ and $\lambda \in \{\|\tilde{\phi}\|_n/2^7, \|\tilde{\phi}\|_n/2^{11}, \|\tilde{\phi}\|_n/2^{15}\}$ for $K = 3$, where $\tilde{\phi}$ is the centered version of ϕ . For solutions from AS-BDT (after convergence declared), the sparsity levels and MSEs under different tuning parameters are summarized in Table S1. The sparsity levels from stochastic primal-dual algorithms are reported in Tables S4 and S5. The number of batch steps fixed within each block is 6 for three batch algorithms and 3 for three stochastic algorithms as in Section 5.2.1. A tolerance of 10^{-4} in the objective value is checked at the end of each cycle over all blocks to declare convergence.



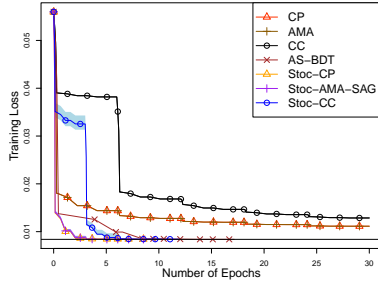
(a) $\rho = 2^{-17}$, $\lambda = \|\tilde{\phi}\|_n/2^7$



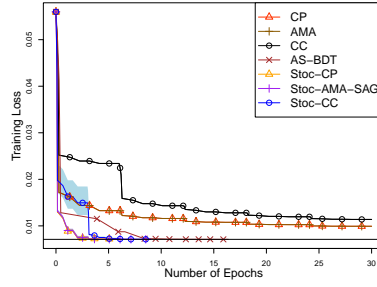
(b) $\rho = 2^{-17}$, $\lambda = \|\tilde{\phi}\|_n/2^9$



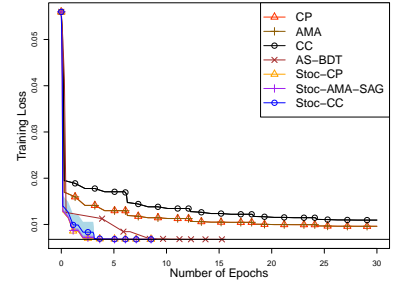
(c) $\rho = 2^{-17}$, $\lambda = \|\tilde{\phi}\|_n/2^{11}$



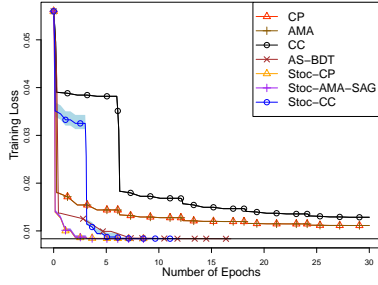
(d) $\rho = 2^{-21}$, $\lambda = \|\tilde{\phi}\|_n/2^7$



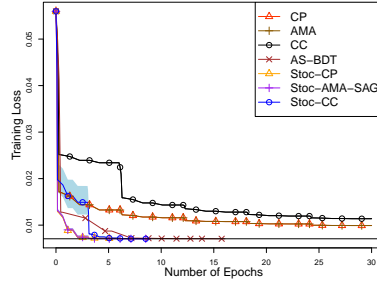
(e) $\rho = 2^{-21}$, $\lambda = \|\tilde{\phi}\|_n/2^9$



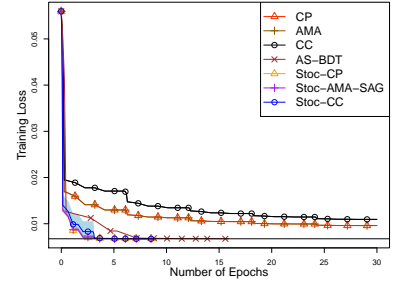
(f) $\rho = 2^{-21}$, $\lambda = \|\tilde{\phi}\|_n/2^{11}$



(g) $\rho = 2^{-25}$, $\lambda = \|\tilde{\phi}\|_n/2^7$



(h) $\rho = 2^{-25}$, $\lambda = \|\tilde{\phi}\|_n/2^9$



(i) $\rho = 2^{-25}$, $\lambda = \|\tilde{\phi}\|_n/2^{11}$

Figure S3: DPAM training in phase shift model with $K = 2$ (up to two-way interactions). The minimal training loss achieved from AS-BDT is given by the black solid line. For the stochastic algorithms, we plot the mean as well as the minimum and maximum training losses across 10 repeated runs.

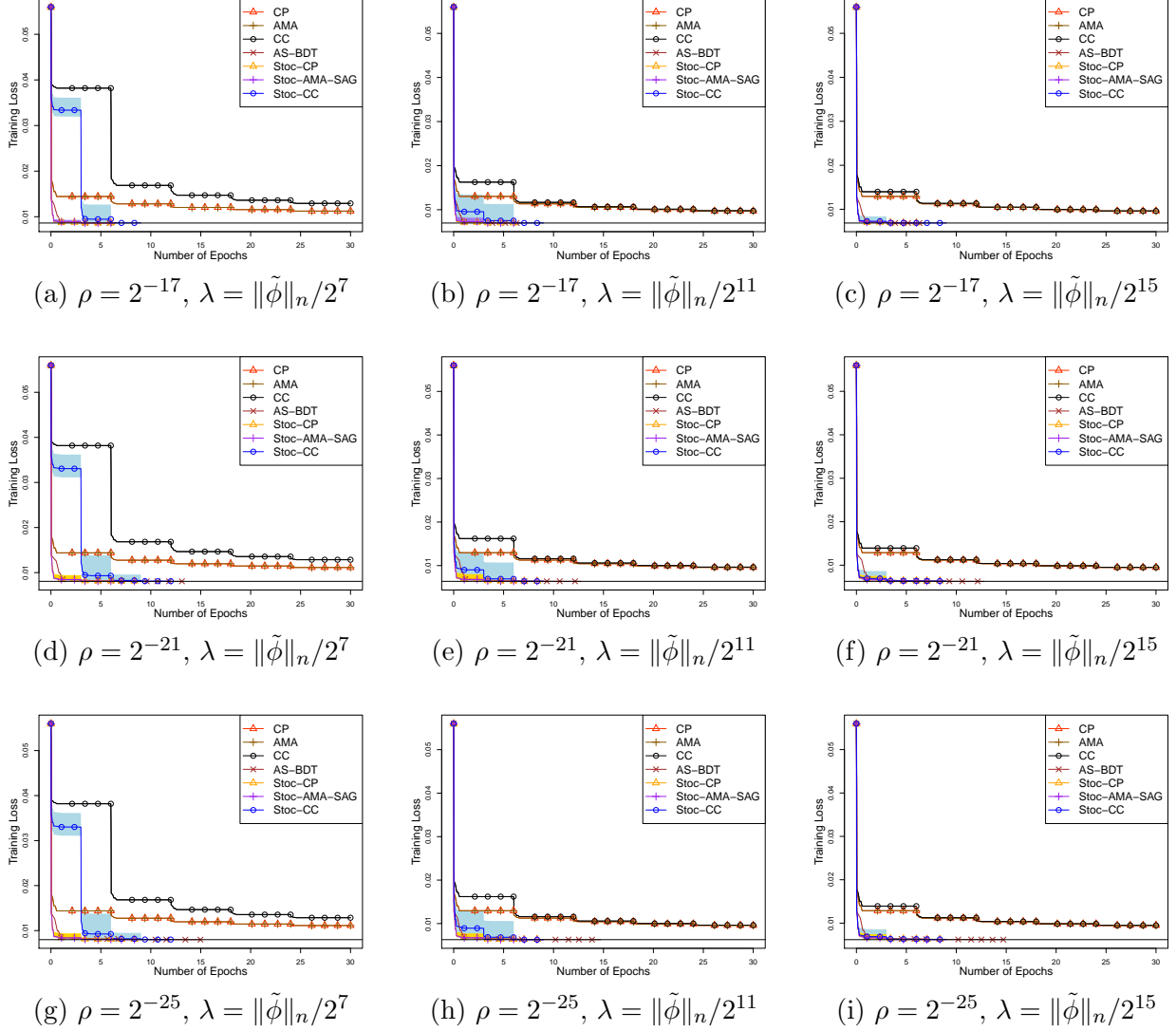


Figure S4: DPAM training in phase shift model with $K = 3$ (up to three-way interactions). The minimal training loss achieved from AS-BDT is given by the black solid line. For the stochastic algorithms, we plot the mean as well as the minimum and maximum training losses across 10 repeated runs.

Table S1: Sparsity and MSEs (in units of 10^{-3}) for the phase shift model.

$K = 2$ (up to two-way interactions)									
$\log_2(\rho^{-1})$	17			21			25		
$\log_2(\lambda^{-1})$	7	9	11	7	9	11	7	9	11
# nonzero blocks	6	8	10	6	9	10	6	8	10
# nonzero coefficients	50	56	58	79	97	96	75	93	96
MSEs (10^{-3})	13.72	13.66	13.66	13.43	13.4	13.40	13.43	13.39	13.40
$K = 3$ (up to three-way interactions)									
$\log_2(\rho^{-1})$	17			21			25		
$\log_2(\lambda^{-1})$	7	11	15	7	11	15	7	11	15
# nonzero blocks	7	13	14	7	14	14	7	13	14
# nonzero coefficients	56	68	69	92	122	122	95	132	132
MSEs (10^{-3})	13.13	13.03	13.03	12.65	12.61	12.61	12.63	12.59	12.59

Note: For $K = 2$, there are 10 blocks from which 4 are main effects and 6 are two-way interactions. There are a total of 640 scalar coefficients. For $K = 3$, there are 14 blocks with 4 additional three-way interactions. There are a total of 4640 scalar coefficients. The MSEs are evaluated on a validation set of $n = 50000$ data points.

V Sparsity levels in numerical experiments

We report the sparsity levels of solutions from stochastic primal-dual algorithms (after the convergences are declared) for the synthetic linear and logistic regression in Section 5 and the phase shift model in Section IV. The sparsity levels for logistic regression on the run-or-walk data in Section 5.2.3 are omitted, because the stochastic primal-dual algorithms may not be declared convergent by the maximum number of epochs attempted. Means and standard deviations (in parenthesis) of the numbers of nonzero blocks and nonzero coefficients across 10 repeated runs are summarized in Tables S2–S5. For easy comparison, we replicate the sparsity levels of solutions from AS-BDT as shown in the main paper.

Table S2: Sparsity for synthetic linear regression

$\log_2(\rho^{-1})$	$\log_2(\lambda^{-1})$	AS-BDT	Stoc-CP	Stoc-AMA-SAG
# Nonzero blocks				
16	6	14	14 (0)	14 (0)
16	8	29	35.2 (1.6)	32 (2.3)
16	10	54	54 (0)	54.1 (0.3)
19	6	14	14 (0)	14 (0)
19	8	54	53.8 (0.4)	52.4 (0.8)
19	10	54	55 (0)	55 (0)
22	6	14	14 (0)	14 (0)
22	8	54	53.8 (0.4)	52.5 (0.7)
22	10	55	55 (0)	55 (0)
# Nonzero coefficients				
16	6	119	131.4 (2.3)	127.60 (1.2)
16	8	195	251.2 (10.6)	226.80 (12.6)
16	10	335	357.2 (1.9)	352.20 (1.2)
19	6	169	183.3 (2.0)	183.00 (2.8)
19	8	670	832.8 (8.5)	842.4 (14.3)
19	10	656	850.5 (5.1)	832.8 (3.9)
22	6	185	209.2 (0.8)	209.50 (0.5)
22	8	841	1157.6 (3.7)	1149.7 (6.7)
22	10	885	1167.5 (2.3)	1163.3 (3.0)

Note: For $K = 2$, there are 55 blocks from which 10 are main effects and 45 are two-way interactions. There are a total of 1175 scalar coefficients. For the underlying regression function (49), 14 of the 55 components are true.

Table S3: Sparsity for synthetic logistic regression

$\log_2(\rho^{-1})$	$\log_2(\lambda^{-1})$	AS-BDT	Stoc-CP	Stoc-AMA-SAG
# Nonzero blocks				
16	6	13	13.9 (0.3)	13.9 (0.3)
16	8	46	48 (0.7)	47.7 (0.7)
16	10	55	55 (0)	55 (0)
19	6	18	16.2 (0.4)	16 (0)
19	8	55	55 (0)	55 (0)
19	10	55	55 (0)	55 (0)
22	6	39	28.7 (0.5)	27.1 (0.7)
22	8	55	55 (0)	55 (0)
22	10	55	55 (0)	55 (0)
# Nonzero coefficients				
16	6	91	92.8 (0.9)	92.6 (1.0)
16	8	226	231.1 (2.1)	230.6 (2.2)
16	10	258	261.3 (1.1)	258.5 (0.7)
19	6	205	182.9 (6.0)	177.9 (2.9)
19	8	658	670.9 (3.6)	665.5 (1.6)
19	10	655	667.8 (1.8)	661.5 (2.5)
22	6	721	542.8 (12.6)	506.4 (16.3)
22	8	1011	1086.5 (3.1)	1073.0 (2.9)
22	10	1020	1098.8 (2.9)	1076.4 (1.3)

Note: For $K = 2$, there are 55 blocks from which 10 are main effects and 45 are two-way interactions. There are a total of 1175 scalar coefficients. For the underlying regression function (49), 14 of the 55 components are true.

Table S4: Sparsity for phase shift model with $K = 2$

$\log_2(\rho^{-1})$	$\log_2(\lambda^{-1})$	AS-BDT	Stoc-CP	Stoc-AMA-SAG
# Nonzero blocks				
17	7	6	6 (0)	6 (0)
17	9	8	10 (0)	10 (0)
17	11	10	10 (0)	10 (0)
21	7	6	6.3 (0.5)	6 (0)
21	9	9	10 (0)	10 (0)
21	11	10	10 (0)	10 (0)
25	7	6	9 (0)	9 (0)
25	9	8	10 (0)	10 (0)
25	11	10	10 (0)	10 (0)
# Nonzero coefficients				
17	7	50	124.2 (8.0)	99.8 (6.1)
17	9	56	147.3 (8.3)	114.9 (6.3)
17	11	58	143.8 (9.7)	113.9 (5.5)
21	7	79	301.2 (29.5)	208.8 (8.9)
21	9	97	484.9 (35.1)	326.0 (13.3)
21	11	96	431.2 (15.7)	325.7 (11.0)
25	7	75	628.3 (1.2)	629.8 (0.4)
25	9	93	639.4 (0.5)	637.9 (0.6)
25	11	96	638.9 (0.6)	637.1 (1.2)

Note: For $K = 2$, there are 10 blocks from which 4 are main effects and 6 are two-way interactions. There are a total of 640 scalar coefficients. For $K = 3$, there are 14 blocks with 4 additional three-way interactions. There are a total of 4640 scalar coefficients.

Table S5: Sparsity for phase shift model with $K = 3$

$\log_2(\rho^{-1})$	$\log_2(\lambda^{-1})$	AS-BDT	Stoc-CP	Stoc-AMA-SAG
# Nonzero blocks				
17	7	7	7 (0)	7 (0)
17	11	13	12 (0)	12.4 (0.7)
17	15	14	14 (0)	14 (0)
21	7	7	8.6 (0.5)	7 (0)
21	11	14	14 (0)	14 (0)
21	15	14	14 (0)	14 (0)
25	7	7	13 (0)	11.6 (0.5)
25	11	13	14 (0)	14 (0)
25	15	14	14 (0)	14 (0)
# Nonzero coefficients				
17	7	56	148.7 (7.4)	113 (4)
17	11	68	169.8 (7.8)	129.7 (3.4)
17	15	69	176.1 (7.7)	139.3 (2.6)
21	7	92	567.8 (58.2)	360.8 (9.4)
21	11	122	764.3 (69.9)	550.7 (10.8)
21	15	122	825.3 (85.9)	553.5 (12.7)
25	7	95	3238.2 (138.0)	2715.3 (376.7)
25	11	132	3535.3 (94.5)	3178.9 (58.9)
25	15	132	3596.4 (86.3)	3182.7 (53.7)

Note: For $K = 2$, there are 10 blocks from which 4 are main effects and 6 are two-way interactions. There are a total of 640 scalar coefficients. For $K = 3$, there are 14 blocks with 4 additional three-way interactions. There are a total of 4640 scalar coefficients.

VI Tuning information

We tune three batch algorithms (Algorithms 1, 2, and S1) and their stochastic versions (Algorithms 3, 4, and S2) in all numerical experiments. In repeated runs for stochastic algorithms, tuning is performed only in the first run. The selected step sizes are then used in all the subsequent runs.

For each algorithm, the step sizes attempted are taken from the set $\{a \times 10^{-k} : a \in \{1, 2, \dots, 9\}, k \in \mathbb{Z}\}$ unless otherwise noted in Table S8. We start from a candidate set $S = \{0.1, 0.2, \dots, 1\}$. The best step size in S which gives the minimal training loss after a given number of epochs is selected. If the best step size is the largest element in S (say 1), modify the candidate set to be $S \leftarrow 10 \cdot S$ (i.e., all elements in S are multiplied by 10). If the best step size is the smallest element (say 0.1), modify the candidate set as $S \leftarrow 0.1 \cdot S$ (i.e., all elements in S are multiplied by 0.1). The procedure is repeated until a non-monotone change of training loss is detected. For example when 0.5 is the best in $S = \{0.1, 0.2, \dots, 1\}$ or 0.1 is the best in both $\{0.1, 0.2, \dots, 1\}$ and $\{0.01, 0.02, \dots, 0.1\}$. To limit the amount of search we restrict the range of step sizes between 0.001 and 100.

For Algorithms S1 and S2, only a single step size τ needs tuning. For primal-dual algorithms (Algorithm 1, 2, 3, and 4), there are two step sizes τ and α . For simplicity, we tune one step size while fixing the other at a preliminary value, and then tune the second step size while fixing the first at the selected value. From our numerical experience, Algorithm 4 (Stoc-AMA) seems to be more sensitive to α than to τ . Hence for Algorithm 4 we first tune α then τ . For the other primal-dual algorithms we first tune τ then α .

In the simulated, multi-block experiments (Sections 5.2.1, 5.2.2, and IV), all inputs are sampled uniformly from $[0, 1]$. For simplicity, tuning is performed with the same step sizes used in all blocks. For the real-data experiments (Section 5.2.3), tuning is performed separately within each block while removing the other blocks (as in single-block experiments). If ignoring any difference in how many times the candidate sets are adjusted, the two procedures roughly have similar costs, because performing one epoch in multi-block experiments has a similar cost as performing single-block epochs across all blocks.

VI.1 Single-block experiments

For the single-block experiments (Figure 1), the first 5 epochs are for tuning, and the results are summarized in Table S6.

Table S6: Step sizes for the single-block experiments.

λ	$\lambda_0(\rho)/4$			$2\lambda_0(\rho)$		
$\log_2(\rho^{-1})$	15	18	21	15	18	21
CP	100,0.8	100,0.8	100,0.8	0.001,100	0.001,100	0.001,100
AMA	100,0.5	100,0.5	100,0.5	0.001,100	0.001,100	0.001,100
CC	100	100	100	0.001	0.001	0.001
Stoc-CP	20,1	20,1	30,0.8	6,6	30,1	5,8
Stoc-AMA-SAG	30,1	30,1	40,1	1,50	0.5,30	0.9,60
Stoc-AMA-SAGA	9,0.7	20,0.6	20,0.6	0.8,30	0.6,30	0.5,30
Stoc-CC	20	20	20	0.001	0.001	0.001

Note: There is one step size τ for CC and Stoc-CC. For primal-dual methods there are two step sizes τ, α , listed from left to right.

VI.2 Multi-block experiments

For the phase shift model (Figure S3 and Figure S4), the first 2 epochs are for tuning. The results are summarized in Table S7.

For the synthetic linear regression model (Figure 2), the first 6 epochs are for tuning. For the synthetic logistic model (Figure 3), the first 10 epochs are for tuning. The corresponding step sizes are summarized in Table S8.

For logistic regression on the run-or-walk data (Figure 4), step sizes are tuned separately within each block as mentioned earlier. The first 10 epochs are for tuning. For conciseness, we only report the step sizes under $\rho = 2^{-23}$ and $\lambda = \|\tilde{Y}\|_n/2^{13}$ in Table S9, which are the tuning parameters with the smallest misclassification rate on the validation set. From Table S9 we observe that the magnitude of step sizes varies widely among the blocks associated with main and two-way effects.

Table S7: Step sizes for phase shift model.

$K = 2$ (up to two-way interactions)									
$\log_2(\rho^{-1})$	17			21			25		
$\log_2(\lambda^{-1})$	7	9	11	7	9	11	7	9	11
CP	20,0.7	20,0.7	20,0.7	20,0.7	20,0.7	20,0.7	20,0.7	20,0.7	20,0.7
AMA	20,0.5	20,0.5	20,0.5	20,0.5	20,0.5	20,0.5	20,0.5	20,0.5	20,0.5
CC	10	10	10	10	10	10	10	10	10
Stoc-CP	0.4,4	0.3,5	0.4,4	0.6,4	0.4,6	0.6,4	0.6,4	0.4,6	0.6,4
Stoc-AMA-SAG	1,0.8	1,0.8	1,0.8	2,0.8	2,0.8	2,0.8	2,0.8	2,0.8	2,0.8
Stoc-CC	1	2	1	1	2	2	1	2	2
$K = 3$ (up to three-way interactions)									
$\log_2(\rho^{-1})$	17			21			25		
$\log_2(\lambda^{-1})$	7	11	15	7	11	15	7	11	15
CP	20,0.6	20,0.6	20,0.6	20,0.6	20,0.6	20,0.6	20,0.6	20,0.6	20,0.6
AMA	20,0.4	20,0.4	20,0.4	20,0.4	20,0.4	20,0.4	20,0.4	20,0.4	20,0.4
CC	10	20	20	10	20	20	10	20	20
Stoc-CP	0.6,4	0.6,4	0.5,8	0.8,4	0.9,4	0.6,9	0.8,4	0.8,4	0.6,9
Stoc-AMA-SAG	2,0.8	2,0.8	1,0.8	2,0.8	2,0.8	2,0.8	2,0.8	2,0.8	2,0.8
Stoc-CC	1	3	0.6	2	3	0.8	2	3	0.8

Note: There is one step size τ for CC and Stoc-CC. For primal-dual methods there are two step sizes τ, α , listed from left to right.

Table S8: Step sizes for synthetic linear and logistic regressions.

Linear regression									
$\log_2(\rho^{-1})$	16			19			22		
$\log_2(\lambda^{-1})$	6	8	10	6	8	10	6	8	10
CP	20,0.2	20,0.2	20,0.2	20,0.2	20,0.2	20,0.2	20,0.2	20,0.2	20,0.2
AMA	20,0.4	20,0.4	20,0.4	20,0.4	20,0.4	20,0.4	20,0.4	20,0.4	20,0.4
CC	10	20	20	10	20	20	10	20	20
Stoc-CP	2,2.5	4,1.5	2,3.5	2,2.5	4,1.5	2,3.5	2,2.5	4,1.5	2,3.5
Stoc-AMA-SAG	3,0.8	10,0.9	3,0.7	4,0.8	20,0.9	4,0.7	4,0.8	20,0.9	4,0.7
Stoc-CC	2	2	2	2	2	2	2	2	2
Logistic regression									
$\log_2(\rho^{-1})$	16			19			22		
$\log_2(\lambda^{-1})$	6	8	10	6	8	10	6	8	10
CP	20,0.4	20,0.2	20,0.2	20,0.4	20,0.2	20,0.2	20,0.4	20,0.2	20,0.2
AMA	10,2	20,0.2	20,0.2	10,2	20,0.2	20,0.2	10,2	20,0.2	20,0.2
CC	10	20	20	10	20	20	10	20	20
Stoc-CP	2,1	2,1	2,1	5,1	5,1	5,1	5,1	6,1	6,1
Stoc-AMA-SAG	5,0.9	3,1	6,0.9	5,0.9	8,0.4	8,0.4	10,0.9	10,0.4	10,0.4
Stoc-CC	4	3	3	4	3	3	4	3	4

Note: There is one step size τ for CC and Stoc-CC. For primal-dual methods there are two step sizes τ, α , listed from left to right. The step size α for Stoc-CP is picked from $\{1, 1.5, 2, 2.5, 3, 3.5, 4\}$.

Table S9: Step sizes for logistic regression on real data with $\rho = 2^{-23}$ and $\lambda = \|\tilde{Y}\|_n/2^{13}$.

Algorithms	CP		AMA		CC	Stoc-CP		Stoc-AMA-SAG		Stoc-CC
Block index	τ	α	τ	α	τ	τ	α	τ	α	τ
1	1	0.2	1	0.2	1	0.07	6	0.4	0.2	0.08
2	1	0.3	1	0.2	1	0.2	1	0.5	0.5	0.07
3	0.6	0.2	0.6	0.1	0.6	0.1	0.9	0.05	1	0.05
4	1	0.5	1	0.4	1	0.04	0.6	0.03	0.4	0.1
5	1	0.8	1	0.6	1	0.1	0.4	0.3	0.3	0.04
6	2	0.5	2	0.4	2	0.5	0.9	0.4	0.3	0.2
1,2	0.7	0.2	0.7	0.2	0.7	0.009	1	0.003	0.04	0.001
1,3	0.1	0.1	0.1	0.1	0.1	0.007	0.01	0.2	0.02	0.003
1,4	0.3	0.07	0.3	0.06	0.3	0.01	0.2	0.03	0.3	0.005
1,5	0.6	0.3	0.6	0.3	0.6	0.01	1	0.4	0.02	0.005
1,6	0.7	0.2	0.7	0.2	0.7	0.03	0.2	0.08	0.3	0.01
2,3	0.3	0.2	0.3	0.1	0.3	0.01	0.09	0.05	0.2	0.004
2,4	1	0.5	1	0.4	1	0.01	2	0.03	0.2	0.006
2,5	1	0.3	1	0.3	1	0.01	0.5	0.02	0.5	0.006
2,6	1	0.2	1	0.2	1	0.06	0.3	0.08	0.3	0.02
3,4	1	0.3	1	0.3	1	0.01	1	0.02	0.7	0.005
3,5	0.3	0.4	0.3	0.3	0.3	0.005	0.3	0.004	0.1	0.002
3,6	0.4	0.3	0.4	0.2	0.4	0.01	0.2	0.06	0.2	0.006
4,5	1	0.3	1	0.2	1	0.03	0.4	0.06	0.4	0.01
4,6	1	0.2	1	0.2	1	0.06	0.3	0.1	0.3	0.03
5,6	1	0.2	1	0.2	1	0.04	0.3	0.1	0.4	0.02

Note: Blocks with indices 1 to 6 refer to main effects of 6 explanatory variables acc_x , acc_y , acc_z , $gyro_x$, $gyro_y$, and $gyro_z$ respectively. Blocks with double indices refer to the corresponding two-way interactions.

VI.3 Recoveries

We perform a check-and-recovery after the update of each block as follows. If the training loss increases rather than decreases, we skip the update for the current block and directly move to the next block. The cost of checking is negligible, and this operation leads to more stable performances (especially for stochastic algorithms). In particular, we find the check-and-recovery useful in the real-data experiments where step sizes are tuned block-wise. Table S10 reports the recovery information of stochastic algorithms in the real-data experiments across 10 repeated runs. From Table S10 we observe that Stoc-CP is more robust against bad step sizes than the other two stochastic algorithms.

Table S10: Recovery for logistic regression on real data.

Total numbers of recoveries									
$\log_2(\rho^{-1})$	18			23			25		
$\log_2(\lambda^{-1})$	6	13	15	6	13	15	6	13	15
Stoc-CC	398	177	169	504	163	167	503	162	167
Stoc-CP	342	42	41	287	42	43	284	42	43
Stoc-AMA-SAG	532	159	161	572	166	132	571	165	133
Numbers of blocks with recoveries									
$\log_2(\rho^{-1})$	18			23			25		
$\log_2(\lambda^{-1})$	6	13	15	6	13	15	6	13	15
Stoc-CC	11	11	10	14	11	10	14	11	10
Stoc-CP	10	5	5	6	5	5	6	5	5
Stoc-AMA-SAG	12	8	8	12	7	6	12	7	6

Note: The counts are collected for stochastic algorithms in 10 repeated runs, each with 80 epochs (corresponding to 16 backfitting cycles with 5 batch steps in each block). There are 21 blocks in total. For example, when $\rho = 2^{-18}$ and $\lambda = \|\tilde{Y}\|_n/2^6$, Stoc-CC has a total of 398 recoveries from 11 different blocks during the 10 repeated runs.

References

- Condat, L. (2013). A primal–dual splitting method for convex optimization involving Lipschitzian, proximable and linear composite terms. *Journal of Optimization Theory and*

- Applications*, 158, 460-479.
- Friedman, J. (1991). Multivariate adaptive regression splines (with discussion). *Annals of Statistics*, 19 , 79–141.
- Hunter, D. R., & Lange, K. (2004). A tutorial on MM algorithms. *American Statistician*, 58 , 30–37.
- Hunter, D. R., & Li, R. (2005). Variable selection using MM algorithms. *Annals of Statistics*, 33 , 1617.
- Li, Z., & Yan, M. (2021). New convergence analysis of a primal-dual algorithm with large stepsizes. *Advances in Computational Mathematics*, 47 , 1–20.
- Parikh, N., & Boyd, S. (2014). Proximal algorithms. *Foundations and Trends in Optimization*, 1 , 127–239.
- Ryu, E. K., & Yin, W. (2022). *Large-Scale Convex Optimization via Monotone Operators*. Cambridge University Press.
- Tseng, P. (1988). Coordinate ascent for maximizing nondifferentiable concave functions. *Technical Report LIDS-P-1840, MIT*.
- Vũ, B. C. (2013). A splitting algorithm for dual monotone inclusions involving cocoercive operators. *Advances in Computational Mathematics*, 38 , 667–681.